Effects of Electron-Vibron Coupling in Fe_4 Single-Molecule Magnet Transport Junctions Using a Density Functional Theory and Model Hamiltonian Approach

by

Alexander McCaskey

B.S., University of Tennessee, Knoxville (2010)

Submitted to the Department of Physics
in partial fulfillment of the requirements for the degree of

Master of Science in Physics

at the

VIRGINIA POLYTECHNIC INSTITUTE AND STATE UNIVERSITY

May 2014

Supervised by .....

Kyungwha Park
Associate Professor

Effects of Electron-Vibron Coupling in Fe_4 Single-Molecule Magnet Transport Junctions Using a Density Functional Theory and Model Hamiltonian Approach

by

Alexander McCaskey

Submitted to the Department of Physics
on April 28, 2014, in partial fulfillment of the
requirements for the degree of
Master of Science in Physics

Abstract

Recent experiments have shown that junctions consisting of individual single-molecule magnets (SMMs) bridged between two electrodes can be fabricated in three-terminal devices, and that the characteristic magnetic anisotropy of the SMMs can be affected by electrons tunneling through the molecule. Vibrational modes of the SMM can couple to electronic charge and spin degrees of freedom, and this coupling also influences the magnetic and transport properties of the SMM. The effect of electron-vibron coupling on transport has been extensively studied in small molecules, but not yet for junctions of SMMs. The goals of this thesis will be two-fold: to present a novel approach for studying the effects of this electron-vibron coupling on transport through SMMs that utilizes both density functional theory calculations and model Hamiltonian construction and analysis, and to present a software framework based on this hybrid approach for the simulation of transport across user-defined SMMs. The results of these simulations will indicate a characteristic suppression of the current at low energies that is strongly dependent on the overall electron-vibron coupling strength and number of molecular vibrational modes considered.

Thesis Supervisor: Kyungwha Park
Title: Associate Professor

Acknowledgments

I would like to first and foremost acknowledge and thank my advisor, Dr. Kyungwha Park. She provided a fascinating and enjoyable project, funding for me to work full-time, and the opportunity to learn from someone with years of experience in the field. I appreciate all the long meetings, the aid and advice, the knowledge I've garnered from her teaching, the opportunity to travel, and her overall patience with me as I've worked to meet our goals. The amount she taught me over the past months extends far beyond the actual physics; I've learned what it takes to be a professional researcher and contributor to the field.

I am so thankful for my family. Mom and Dad, without you I would not be in the position I am today. Your love and support throughout all this has been absolutely crucial to my success, and I'll never forget it. Tyler, thanks for always being there, talking Packers football, and just being a great friend and brother. Becca, your love and support over the past year has propelled me forward, and kept me sane. It's hard to imagine being able to finish this work without you always being there for me. I also want to thank my grandparents, whose constant encouragement, support, and advice throughout my time in graduate school has not gone unnoticed, and is so appreciated.

I wouldn't be here without the support and experience I got from my mentors, friends, and colleagues at ORNL. I want to especially acknowledge David Bernholdt, Travis Humble, and Cindy Sonewald. They presented me with great opportunities for success, helped me along when I needed it, or just provided a friendly conversation during the time I spent there.

A special acknowledgement goes to my friend and colleague, Jay Billings. You took in and mentored a guy who had nothing but a willingness to learn and work hard, you provided opportunities I otherwise would never have had, and through it all you became a great and valued friend.

Contents

List of Figures

List of Tables

Introduction

Single-molecule magnets (SMMs) are unique molecular systems that exhibit a large ground state magnetic moment coupled with a large uniaxial magnetic anisotropy. The combined effort of these two features leads directly to a bistable ground state at low temperatures, which, coupled with the fact that their size is on the order of a nanometer, provides a key mechanism for the construction of dense information storage schemes. Furthermore, certain intrinsic transverse effects can give rise to a mixing of oppositely oriented magnetic states, giving rise to an effect known as macroscopic magnetic quantum tunneling. It is this superposition of states that could prove invaluable to future quantum computing architectures.

To take advantage of these, as well as many other unique properties, future applications will need some way to manipulate and control SMMs. Studies of electron transport across these molecules, as well as experimentally characterizing their unique current-voltage characteristics, are therefore of prime importance. It is known that this transport can couple to a number of molecular degrees of freedom, such as spin or vibrational modes, and this coupling directly influences the current across the molecule.

Transport across SMMs has been extensively studied both theoretically and experimentally, with most theoretical studies ignoring these external coupling effects due to the complexity they introduce. Additionally, most theoretical studies approach the problem of transport across SMMs in one of two ways: (1) using density functional theory (DFT) and non-equilibrium Green's functions, or (2) model Hamiltonians coupled with a master equation approach for eigenstate occupation probabilities.

The goal of this work is to study the transport properties for an iron based SMM

(known as Fe_4) in the presence of coupling between electronic and vibrational degrees of freedom. We will approach this problem by utilizing a novel approach that takes from the best of both techniques discussed above. Specifically, we will use DFT-calculated parameters, such as the strength of the electron-vibron coupling, in our model Hamiltonian analysis.

This work will begin with an overview of SMMs, including a discussion of their defining features and model Hamiltonian. Ch. 2 will discuss DFT and a method that uses it in an iterative manner to compute molecular equilibrium geometries, which will prove invaluable for computing the effects of electron-vibron coupling. Then we will detail the overall theory behind electron transport in Ch. 3. We will discuss transport in the absence of molecular vibrations first, and then build up a theory that incorporates vibrational coupling by approximating the nuclear wave functions as an uncoupled set of harmonic oscillators. Ch. 4 will detail an extensible and scalable application we have written for simulations of electron transport across SMMs, called *SMMSim*. Lastly, in Ch. 5 we will show our results for SMMSim simulations of transport across Fe_4, which will indicate a characteristic low-bias suppression of the current that cannot be modified by the application of a gate voltage.

Chapter 1

Single-Molecule Magnets

Single-molecule magnets (SMMs) are organo-metallic molecules that form crystalline structures and exhibit a number of unique properties that allow them to effectively straddle the quantum and classical worlds [9], and therefore provide a prime test-bed for the analysis of macroscopic quantum phenomena. With a large ground state magnetic moment, and an intrinsic resistance to magnetic relaxation below certain temperatures, these molecules provide a promising avenue for the construction of super-dense information storage schemes. Additionally, under the correct circumstances, the magnetic relaxation of SMMs can be aided by quantum tunneling effects, a feature that could pave the way to future quantum computing architectures. This chapter will detail the unifying features of molecular magnetism, as well as delve into a quantitative description of the physics underlying current SMM research efforts.

1.1 Features of Single-Molecule Magnets

The two fundamental characteristics all SMMs exhibit are a large ground state magnetic moment coupled with a relatively large uniaxial magnetic anisotropy. This anisotropy defines an easy-axis for the magnetization of the molecule, and leads directly to a set of magnetic levels whose degeneracy is lifted even in the absence of external magnetic fields. This *zero-field splitting* has the effect of separating the first excited magnetic level from the ground magnetic level, with $|\pm M\rangle$ levels degener-

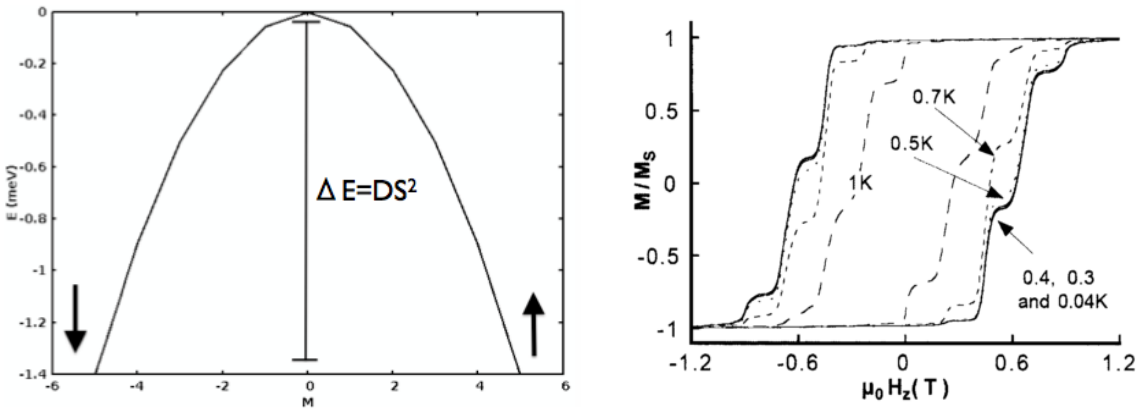

(a) (b)

Figure 1-1: Energy versus magnetic level M (a) and Mn_{12} hysteresis [29] plot (b) showing the key features of SMMs: a parabolic energy spectrum with magnetic anisotropy energy barrier that suppresses magnetic relaxation at low temperatures, and a magnetic hysteresis that shows magnetic relaxation aided by quantum tunneling due to transverse effects.

ate. This leads to a parabolic dependence of the SMM energy spectrum on the spin projection along the easy-axis, M, which gives rise to an effective energy barrier to reverse its magnetic moment (see Fig. 1-1a). Above a temperature greater than the zero-field splitting, the magnetization of the molecule can relax due to thermal effects alone; the ambient thermal energy is high enough for the molecule to overcome this barrier and flip its magnetic state. However, below this temperature, the reversal of the magnetic moment becomes exponentially suppressed, and the orientation of the molecule's spin magnetic moment is relaxed. This bistability of the molecule's magnetic state is an important characteristic for the construction of super-dense information storage schemes, and is dependent on the strength of the molecule's overall magnetic anisotropy.

Even at low temperatures, where there is not enough ambient thermal energy, the magnetic relaxation of the molecule can still occur due to quantum tunneling of the magnetization. This tunneling is driven by transverse magnetic fields and/or the molecule's intrinsic transverse magnetic anisotropy. Without these transverse terms, the magnetic state of the molecule is well defined from the spin projection along the easy-axis, i.e. the eigenvectors $|\pm M\rangle$ of S_z. However, when these effects are present,

the magnetic state or eigenstate of the molecule becomes a superposition of the M levels, which are nearly degenerate across the energy barrier.

The experimentally observed quantum tunneling of magnetization for the Mn_{12} SMM (the first SMM synthesized) is shown in Fig. 1-1b, which shows a plot of the molecule's magnetization versus external magnetic field strength in the direction of the easy-axis. This plot exhibits a clear *hysteresis*, an effect encountered in classical ferromagnetic materials whereby the system is in the metastable magnetic state caused by defects and magnetic domains, and thus leads to the current magnetic state having a clear dependence on the past magnetic configuration of the system. The SMM hysteresis plot at low temperatures exhibits nearly discontinuous jumps at very specific values of the magnetic field, and these steps are due to the system's magnetic state tunneling between almost degenerate magnetic levels with opposite spin directions.

1.2 Model Hamiltonian

The exact Hamiltonian of a SMM can be constructed by considering the contributions from individual magnetic ions present in the molecule. However, this tends to be computationally infeasible for large systems, because the size of the Hilbert space grows exponentially with the addition of each atomic spin [29]. An effective Hamiltonian, known as the *giant spin Hamiltonian*, treats the molecule as a system with a single, large magnetic moment, and explains most of the observed experimental features in crystals of SMMs.

1.2.1 Giant Spin Hamiltonian

The SMM Hamiltonian that captures all the features discussed in Sec. 1.1 can be written as follows

$$\mathcal{H}_{SMM} = \mathcal{H}_0 + \mathcal{H}_T, \tag{1.1}$$

where $\mathcal{H}_0$ and $\mathcal{H}_T$ are the diagonal and off-diagonal (transverse) terms respectively, and are given by

$$\mathcal{H}_0 = -DS_z^2 - BS_z^4 - g\mu_B S_z H_z, \tag{1.2}$$

$$\mathcal{H}_T = E(S_x^2 - S_y^2) + C(S_+^4 + S_-^4) - g\mu_B S_x H_x - g\mu_B S_y H_y. \tag{1.3}$$

Here, S_x, S_y, and S_z are the components of the molecule's spin operator $\mathbf{S}$, D and B, both greater than zero, are the magnetic anisotropy constants in the direction of the easy-axis, and the terms containing the components of the external magnetic field are the familiar Zeeman splitting terms, $g\mu_B\mathbf{S}\cdot\mathbf{H}$, with g being the Lande factor, and μ_B the Bohr magneton. The first two terms of $\mathcal{H}_T$ govern the transverse magnetic anisotropy of the molecule, and exist only under certain molecular symmetries. The second order transverse anisotropy, with strength E, is present when the molecule exhibits rhombic symmetry, while the fourth order term, with strength C, arises from tetragonal symmetry [4].

In the absence of transverse fields and anisotropy (i.e. $\mathcal{H}_T = 0$) $\mathcal{H}_{SMM}$ is purely diagonal and commutes with the S_z operator. Therefore, we can enumerate the eigenstates of $\mathcal{H}_0$ with the eigenstates of the S_z operator, $|\pm M\rangle$, where $M = -S, -S+1, \ldots, S-1, S$. The eigenvalues of the SMM Hamiltonian are then $E(M) = -DM^2 - BM^4 - g\mu_B H_z M$. Fig. 1-1a shows these energies as a function of the spin projection M, with no external field in the z-direction. Furthermore, it shows the magnetic anisotropy energy barrier to overcome relaxation of magnetic moment, which for integer S, can be shown to be $\Delta E = DS^2$.

It should be noted, that in this $\mathcal{H}_T = 0$ scenario, there can be no magnetic quantum tunneling. Without off-diagonal terms in $\mathcal{H}_{SMM}$ there can be no mixing of different M levels.

1.2.2 Effect of External Easy-Axis Field

Now let's consider ramping up an external magnetic field in the direction of the molecule's easy-axis. As seen in Fig. 1-2, increasing H_z lifts the degeneracy between $|\pm M\rangle$, where states with $M > 0$ decrease in energy, and states with $M < 0$ increase

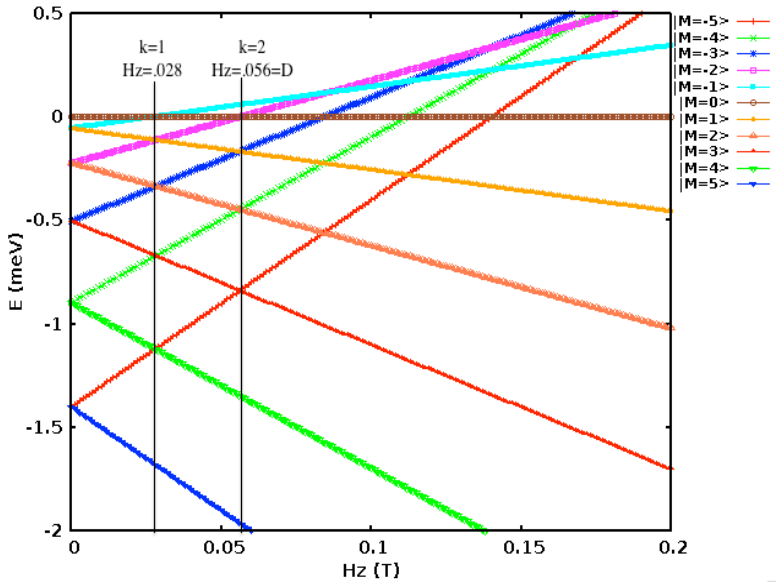

Figure 1-2: Energy Spectrum of Fe_4 with a variable magnetic field. *Generated by SMMSim.*

in energy. As the field further increases, the energies become once again doubly degenerate, but with differing M levels. This occurs at very specific values of the magnetic field, called *resonance fields*. From the Hamiltonian given in Eq. 1.2, one can show that these resonances occur at fields $H_k = \frac{kD}{g\mu_B}$, where $k = |M + M'|$, with M, M' labeling the intersecting magnetic states. With no transverse effects, these resonances simply pertain to level crossings: no tunneling occurs. But when a transverse external field is applied, or the molecule exhibits transverse magnetic anisotropy, the situation changes immensely.

1.2.3 Magnetic Quantum Tunneling

When $\mathcal{H}_T \neq 0$ and off-diagonal terms exist in the molecule's overall Hamiltonian, the presence of the transverse terms lifts the degeneracy of the M levels, leading to the formation of an energy gap in the level crossings discussed above, and thus a finite probability that tunneling of the magnetic states can occur. Fig. 1-3 shows a blown up view of one of these level crossings in the presence of these transverse terms. It depicts the energy gap, denoted with a Δ, and shows that for a large enough gap, the system will tend to remain on a given energy curve as the field is increased, thus

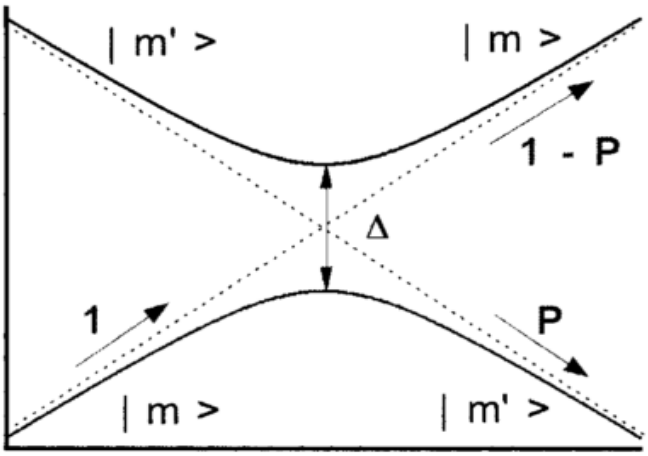

Figure 1-3: Blown up view of a typical level crossing in Fig. 1-2. For $\mathcal{H}_T \neq 0$ an energy gap occurs and leads to a finite probability the system's spin state will reorient itself.

reorienting the overall magnetic state. If the gap is small enough, the system can effectively jump across this energy gap, and therefore remain in the current magnetic state.

By approximating these crossings as an individual two-level system, we can apply the Landau-Zener model [30] of quantum tunneling and the familiar adiabatic approximation [23] to compute the probability that tunneling of the magnetization will occur. With a time-varying external field and ignoring effects due to transverse anisotropy, the probability of a spin flip can be shown to be [29]

$$P_{M,M'} = 1 - \exp\left[- \frac{\pi \Delta^2_{k=M+M'}}{2g\hbar\mu_B |M - M'| (dH_z/dt)} \right], \tag{1.4}$$

and is dependent on the *tunnel splitting* parameter [4],

$$\Delta_k = \frac{2D}{(2S-k-1)^2} \sqrt{\frac{2S}{k!}(2S-k)!} \left(\frac{g\mu_B}{2DS} H_T \right)^{2S-k}, \tag{1.5}$$

with $H_T = \sqrt{H_x^2 + H_y^2}$. Clearly, Δ_k can be adjusted through the application of a field transverse to the easy-axis of the molecule, and the larger the tunnel splitting parameter, the larger the probability that the system will tunnel from a negative magnetic state to a positive one, an effective reversal of the magnetic moment of the SMM.

The hysteresis plot in Fig. 1-1b also shows this tunneling behavior. At the resonance fields labelled by k, the magnetization appears to relax faster, corresponding to large jumps in the plot.

1.3 Fe_4

Now that we have elaborated the unique features of single-molecule magnetism, such as a large uniaxial magnetic anisotropy and the ability for the magnetic state of the system to tunnel, we now turn our focus to the family of SMMs that is the focus of this thesis: Tetrairon(III) SMMs, and specifically, $Fe_4(OCH_3)_6(dpm)_6$ (hereafter abbreviated Fe_4), where (Hdpm) is dipivaloylmethane [1]. Fig. 1-4 shows the overall molecular structure of this SMM. Each iron ion in the SMM has a spin $S = 5/2$, and the spin magnetic moments of the three outer iron ions interact antiferromagnetically with the center iron ion. This spin configuration leads to the characteristically large total spin value of $S = 5$. The geometry of this molecule has a crystalline two-fold (C_2) symmetry, with the symmetry axis running through the center two iron ions [1]. Experimental studies from [1] have shown Fe_4 to have a uniaxial magnetic anisotropy parameter $D = -.056$ meV, and a magnetic reversal energy barrier to be $\Delta E = 1.4$ meV.

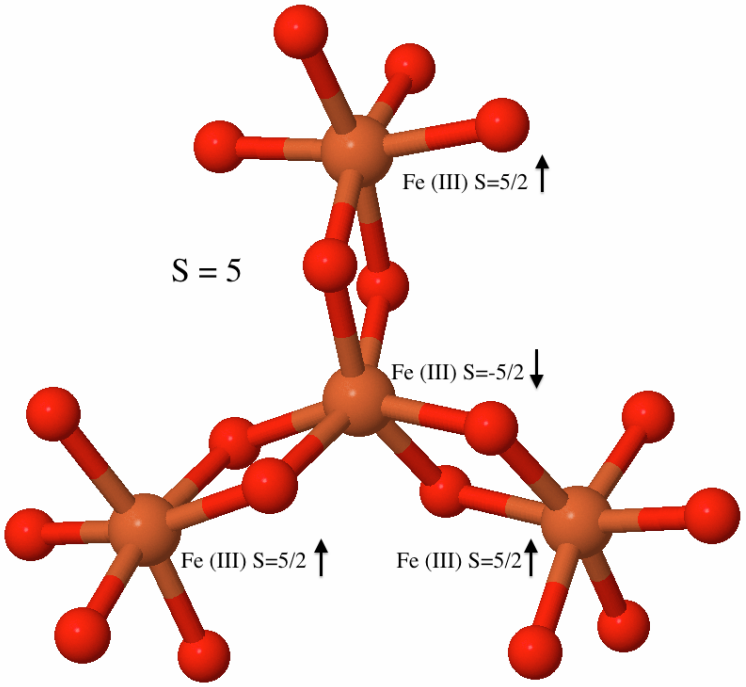

(a) Core Fe_4 structure exhibiting spin structure leading to S=5 total spin. The color scheme is as follows: Fe (orange) and O (red).

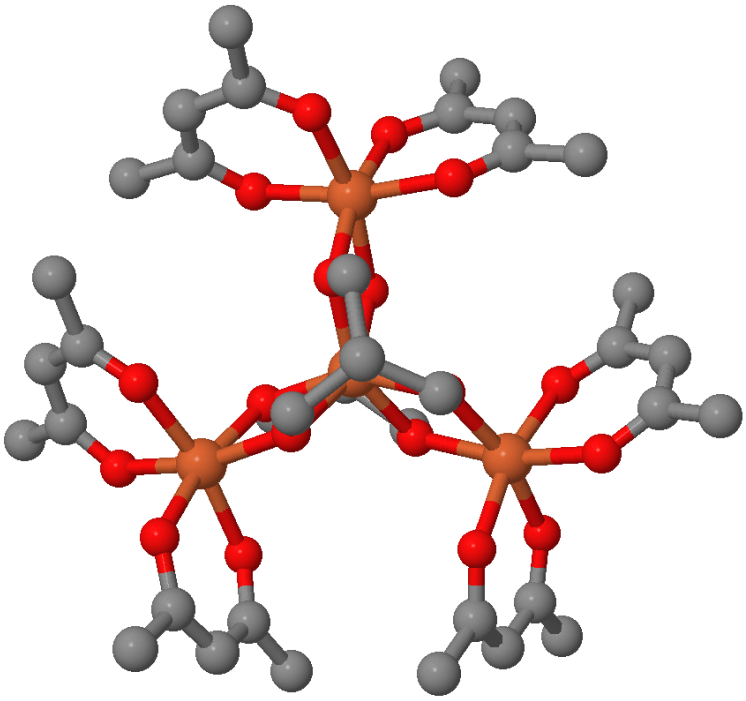

(b) Fe_4 with the color scheme: Fe (orange), O (red), and C (red). Hydrogen atoms and phenyl rings are not shown.

Figure 1-4: Fe_4 Single-Molecule Magnet

Chapter 2

Density Functional Theory

The development of quantum theory and its prize result the Schrödinger equation has revolutionized modern society and technology. It is a theory that accurately predicts the evolution of microscopic systems by introducing a single function, called the *wave function*, that encapsulates the state of the system. This function provides the entirety of information one can know about the system's observables. With an initial wave function known, the state at all times is found through the following eigenvalue equation (Schrödinger equation)

$$-i\hbar\frac{\partial}{\partial t}\psi = \mathcal{H}\psi \tag{2.1}$$

where the wave function is denoted with the greek letter ψ and $\mathcal{H} = \mathcal{T} + \mathcal{V}$ is the system's Hamiltonian (the overall energy content of the system, composed of both kinetic and potential energy).

The beauty of Eq. 2.1 is found in its overall simplicity. Unfortunately, this simplicity quickly fades when analyzing systems of many quantum constituents, such as the electronic structure of a polyatomic system (the primary system studied in this thesis) under appropriate approximations. One such approximation, the *Born Approximation* allows the separation of nuclear and electronic degrees of freedom, due to the fact the mass of the proton is nearly 2000 times larger than that of the electron. Under this approximation, Eq. 2.1 can be solved for the ground state configuration

of the nuclear wave function, which can then be used in the solution of the electronic wave function. This electronic wave function can be expressed as $\Psi(\mathbf{x}_1, \mathbf{x}_2, \cdots, \mathbf{x}_N)$, where each $\mathbf{x}_i \equiv \{\mathbf{r}_i, s_i\}$ represents the electron's position and spin. Inserting the appropriate Hamiltonian for this many electron case, one finds that Eq. 2.1 becomes

$$[\mathcal{H}_e + \mathcal{H}_{ee}]\Psi(\mathbf{x}_1, \mathbf{x}_2, \cdots, \mathbf{x}_{N_e}) = E\Psi(\mathbf{x}_1, \mathbf{x}_2, \cdots, \mathbf{x}_{N_e}), \tag{2.2}$$

for

$$\mathcal{H}_e = -\frac{\hbar^2}{2m}\sum_i^{N_e} \nabla_i^2 - \sum_{i,j}^{N_e,N_n} \frac{eZ_j}{|\mathbf{r}_i - \mathbf{R}_j|} \tag{2.3}$$

which is simply a sum of single-electron Hamiltonians, and

$$\mathcal{H}_{ee} = \sum_{i<j}^{N_e} \frac{e^2}{|\mathbf{r}_i - \mathbf{r}_j|}, \tag{2.4}$$

which quantifies the electron-electron Coulomb interactions. Here N_e and N_n are the number of electrons and nuclei, respectively, and E represents the overall energy of the system.

The solution of Eq. 2.2 is a formidable, and often times impossible, task due to the electron-electron interactions present in Eq. 2.4. Many methods have been concocted over the past half century to overcome this problem and present of a solution of the Schrödinger equation for any number of constituent, interacting parts. The most notable among these are the Thomas-Fermi and Hartree-Fock methods, and the Ritz variational [23] and configuration interaction [27] methods. All of these have proven invaluable to the solution of Eq. 2.2, however none of them provide the generality, flexibility, and scalability of density functional theory (DFT).

2.1 Early Development

2.1.1 Hartree Approximation

Developed soon after the discovery of the Schrödinger equation in the 1920s, the Hartree approximation attempts to solve the monoatomic many-electron system by assuming the wave function is a product of single electron wave functions $\Psi(1, \cdots, N) = \phi_1(1)\phi_2(2)\cdots\phi_N(n)$, where $\phi_i(i) = \phi_i(\mathbf{x}_i)\xi_i(s_i)$ (composed of both spatial and spin parts). The primary flaw of this approximation is that the decomposed many-electron state is not antisymmetric. To partially fulfill the requirement that each electron obey fermion statistics, each ϕ_i must be distinct and all must be orthogonal to each other [23]. Minimizing the energy of the system using the variational principle subject to the constraint that all single-electron orbitals are normalized yields the *Hartree equations*

$$\left(-\frac{\hbar^2}{2m}\nabla_i^2 - \frac{Ze^2}{r_i} + V_i(\mathbf{x}_i)\right)\phi_i(\mathbf{x}_i) = \epsilon_i\phi_i(\mathbf{x}_i) \tag{2.5}$$

with

$$V_i(\mathbf{x}_i) = \sum_{i\neq j}\int d^3x_j \frac{e^2}{|\mathbf{x}_i - \mathbf{x}_j|}|\phi_j(\mathbf{x}_j)|^2. \tag{2.6}$$

Since Eq. 2.6 contains all $j \neq i$ orbitals, the Hartree equations must be solved *self-consistently*. By starting with an initial set of orbitals ϕ_i, Eq. 2.6 can be evaluated and used in Eq. 2.5, which can then be solved for the new set of ϕ_i. This new set is used again in the evaluation of the new potential and the Hartree equations are solved again. This process is continued iteratively until the desired convergence criterion are reached [23]. The product of the converged orbitals then forms the ground state configuration of the many-electron system under study, and, using Eqs. 2.5 and 2.6, the ground state energy can be expressed as

$$E = \sum_{i=1}^{N}\epsilon_i - \sum_{i<j}\int d^3x d^3y \frac{e^2}{|\mathbf{x} - \mathbf{y}|}|\phi_i(\mathbf{x})|^2|\phi_j(\mathbf{y})|^2, \tag{2.7}$$

where ϵ_i is simply the single-electron energy.

2.1.2 Hartree-Fock Approximation

Like the Hartree approximation, the Hartree-Fock approximation attempts to find the ground state configuration for a many-electron system using the variational principle. However, the difference lies in the initial ansatz. Hartree-Fock assumes that the many-electron wave function takes the form of a *Slater determinant*

$$\Psi(1,2,\cdots,N) = \frac{1}{\sqrt{N!}} \begin{vmatrix} \phi_1(1) & \cdots & \phi_1(N) \\ \vdots & & \vdots \\ \phi_N(1) & \cdots & \phi_N(N) \end{vmatrix}, \tag{2.8}$$

which inherently obeys the Pauli Exclusion principle due to the antisymmetry of the determinant (swapping rows or columns introduces an overall factor of -1). The energy of this many-electron system is just the expectation value of the Hamiltonian with respect to this antisymmetric state, and can be written as

$$E = \langle \Psi | \mathcal{H} | \Psi \rangle = \sum_{i=1}^{N} H_i + \frac{1}{2} \sum_{i,j=1}^{N} (J_{ij} - K_{ij}) \tag{2.9}$$

where H is simply the expectation value of Hamiltonian with respect to the i^{th} orbital, and J and K are the Coulomb and exchange integrals, respectively. They are given explicitly by [19]

$$H_i = \int \phi_i^*(\mathbf{x})[-\frac{\hbar^2}{2m}\nabla^2 + v(\mathbf{x})]\phi_i(\mathbf{x})d\mathbf{x} \tag{2.10}$$

$$J_{ij} = \int\int \phi_i(\mathbf{x}_1)\phi_i^*(\mathbf{x}_1)\frac{e^2}{|\mathbf{x}_2 - \mathbf{x}_1|}\phi_j^*(\mathbf{x}_2)\phi_j(\mathbf{x}_2)d\mathbf{x}_1 d\mathbf{x}_2 \tag{2.11}$$

$$K_{ij} = \int\int \phi_i^*(\mathbf{x}_1)\phi_j(\mathbf{x}_1)\frac{e^2}{|\mathbf{x}_2 - \mathbf{x}_1|}\phi_i(\mathbf{x}_2)\phi_j^*(\mathbf{x}_2)d\mathbf{x}_1 d\mathbf{x}_2 \tag{2.12}$$

where $v(\mathbf{x})$ is the potential arising from the nuclei. By constraining the orbitals to be orthonormal and performing the functional minimization of Eq. 2.9 with respect to ϕ_i^*, and with the appropriate Lagrange multiplier, we find that the orbitals obey

the following relation

$$\hat{F}\phi_i(\mathbf{x}) = \Big[-\frac{\hbar^2}{2m}\nabla^2 + v + \hat{j} - \hat{k} \Big]\phi_i(\mathbf{x}) = \sum_{j=1}^{N} \epsilon_{ij}\phi_j(\mathbf{x}) \tag{2.13}$$

with the matrix of Lagrange multipliers ϵ_{ij} that are, in general, complex, and the operators $\hat{j}$ and $\hat{k}$ acting accordingly

$$\hat{j}(\mathbf{x}_1)\phi_i(\mathbf{x}_1) = \sum_{k=1}^{N} \int \phi_k^*(\mathbf{x}_2)\phi_k(\mathbf{x}_2)\frac{e^2}{|\mathbf{x}_2 - \mathbf{x}_1|}\phi_i(\mathbf{x}_1)d\mathbf{x}_2 \tag{2.14}$$

$$\hat{k}(\mathbf{x}_1)\phi_i(\mathbf{x}_1) = \sum_{k=1}^{N} \int \phi_k^*(\mathbf{x}_2)\phi_i(\mathbf{x}_2)\frac{e^2}{|\mathbf{x}_2 - \mathbf{x}_1|}\phi_k(\mathbf{x}_1)d\mathbf{x}_2. \tag{2.15}$$

As seen in the Hartree approximation discussed in the previous section, since the Fock operator contains all other orbital wave functions, one must solve Eq. 2.13 in a self-consistent manner. An initial set of orbitals must be supplied and used to solve the Hartree-Fock equations in an iterative way, until the desired convergence is achieved. With the solution orbitals acquired, one can construct the ground state wave function as the prescribed Slater determinant Eq. 2.8. The ground state energy can be found by noticing that the expectation value of the Fock operator with respect to each of the orbitals is

$$\langle\phi_i|\,\hat{F}\,|\phi_i\rangle = \epsilon_{ii} = \epsilon_i = H_i + \sum_{j=1}^{N}(J_{ij} - K_{ij}), \tag{2.16}$$

so that the sum of all orbital energies is

$$\sum_{i=1}^{N}\epsilon_i = E + \frac{1}{2}\sum_{i,j=1}^{N}(J_{ij} - K_{ij}) = E + V_{ee}, \tag{2.17}$$

with E the same as 2.9 and V_{ee} the electron-electron exchange energy. So, finally, the minimized energy can be written as $E = \sum_{i=1}^{N}\epsilon_i - V_{ee} + V_{nn}$, where V_{nn} is the nuclear interaction energy.

2.1.3 Thomas-Fermi Model

The work of Llewellwyn Thomas and Enrico Fermi in 1927 provided a simple, albeit inaccurate, framework for the solution of the many-electron Schrödinger equation. Due to its poor predictions and inaccuracy for molecules and other large systems, it was largely viewed as a novel, yet oversimplified, model. However, its true power lies in the fundamental shift in thinking it brought about regarding the problem of molecular electronic structure calculations. Its key insight was the elevation of the the system's electron density above the molecular wave function in the solution of the system. By expressing the quantities of interest as a functional of the electron density, one can simplify the solution of Schrödinger's equation to that of a functional minimization with respect to the density. These ideas lead directly to the insights by Hohenberg and Kohn which are discussed in Sec. 2.2.

There are two assumptions inherent to the Thomas-Fermi model: (1) electrons are distributed uniformly in a space which is divided into many small cells containing a different number of electrons ΔN, and (2) there is an effective potential that is determined by the nuclear charge and electron distribution [19]. From these assumptions, let us first find the local density n of electrons in a small cell with volume ΔV. The total energy ΔE and the number of electrons ΔN in the cell are given by

$$\Delta E = \frac{8\pi}{5}\left(\frac{2m}{\hbar^2}\right)^{\frac{3}{2}} \Delta V \epsilon_F^{\frac{5}{2}} \tag{2.18}$$

and

$$\Delta N = \frac{8\pi}{3}\left(\frac{2m}{\hbar^2}\right)^{\frac{3}{2}} \Delta V \epsilon_F^{\frac{3}{2}} \tag{2.19}$$

where ϵ_F is the Fermi energy. Upon eliminating the Fermi energy from these relations, one can show that the energy for a single cell as a function of the electron density $n(\mathbf{r}) = \Delta N/\Delta V$ is

$$\Delta E = \frac{3\hbar^2}{10m}\left(\frac{3}{8\pi}\right)^{\frac{2}{3}} V\left(\frac{\Delta N}{\Delta V}\right)^{\frac{5}{3}}. \tag{2.20}$$

By adding up all energy contributions from all cells, letting the volume of the cell go to zero, and collecting constants (C), we arrive at an expression for the kinetic energy

as a functional of the electron density

$$T[n] = C \int n^{\frac{5}{3}}(\mathbf{r}) d\mathbf{r}. \tag{2.21}$$

The total Thomas-Fermi energy functional is then the sum of this kinetic functional, and the electron-nuclei energy functionals

$$E[n(\mathbf{r})] = C \int n^{\frac{5}{3}}(\mathbf{r}) - Z \int \frac{n(\mathbf{r})}{\mathbf{r}} d\mathbf{r} + \frac{1}{2} \int \int \frac{n(\mathbf{r}_1) n(\mathbf{r}_2)}{|\mathbf{r}_1 - \mathbf{r}_2|} d\mathbf{r}_1 d\mathbf{r}_2. \tag{2.22}$$

With this energy functional, we can find the ground state energy of the system being studied by minimizing the functional under the constraint $N = \int n(\mathbf{r}) d\mathbf{r}$, which produces (here μ is the Lagrange multiplier)

$$\mu = \frac{5}{3} C n^{\frac{2}{3}}(\mathbf{r}) - \frac{Z}{r} - \int \frac{n(\mathbf{r})}{|\mathbf{r} - \mathbf{r_2}|} d\mathbf{r_2}. \tag{2.23}$$

Solving Eq. 2.23 for the electron density and inserting back into the energy functional in Eq. 2.22 produces the ground state energy of the many-electron system being studied.

2.2 The Theorems of Hohenberg and Kohn

The work of Pierre Hohenberg and Walter Kohn in 1964 [12], culminating in two theorems regarding the electron density of a many-electron system, successfully generalized the work discussed in Sec. 2.1. It showed that knowledge of the electron density uniquely determines the ground state energy and wave function of a given polyatomic Hamiltonian.

The importance of the electron density is encapsulated in the first Hohenberg-Kohn theorem: *Within an additive constant, the external potential $v(\mathbf{r})$ is completely determined by the electron density $n(\mathbf{r})$* [19]. Since the electron density uniquely determines the external potential and the total number of electrons, we can construct

the total energy as a functional of the density in a similar manner to Sec. 2.1.3

$$E[n] = T[n] + V_{ne}[n] + V_{ee}[n] = \int n(\mathbf{r})v(\mathbf{r})d\mathbf{r} + F_{HK}[n] \tag{2.24}$$

where

$$F_{HK}[n] = T[n] + V_{ee}[n]. \tag{2.25}$$

F_{HK} is the crucial piece of the total energy functional, in that it contains the physics inherent to the electron-electron interactions. It contains both the classical and the non-classical part of the energy functional, in that it models the effects due to the Pauli exclusion principle, as well as any other correlations between the electrons.

The second of the Hohenberg-Kohn theorems provides the means to compute the ground state configuration of the system by minimizing the energy functional with respect to the electron density. The theorem states that *for a trial density* $\tilde{n}(\mathbf{r})$ *such that* $\tilde{n}(\mathbf{r}) \geq 0$ *and* $\int \tilde{n}(\mathbf{r})d\mathbf{r} = N$, $E_0 \leq E[\tilde{n}]$ [19], where E_0 is the ground state energy and $E[\tilde{n}]$ is the functional in Eq. 2.24. Since the trial density uniquely defines its own potential, Hamiltonian, and wave function, we know that

$$\langle \Psi | \, \mathcal{H} \, | \Psi \rangle = \int \tilde{n}(\mathbf{r})v(\mathbf{r})d\mathbf{r} + F_{HK}[\tilde{n}] = E[\tilde{n}] \geq E[n]. \tag{2.26}$$

Using this theorem, we can minimize the energy functional, subject to the constraint that the number of electrons remain N, to produce the primary equation in density functional theory

$$\mu = \frac{\delta E[n]}{\delta n(\mathbf{r})} = v(\mathbf{r}) + \frac{\delta F_{HK}[n]}{\delta n(\mathbf{r})} \tag{2.27}$$

where μ is the chemical potential and enters in here as a Lagrange multiplier corresponding to the particle number constraint. The beauty of density functional theory lies in this equation. This equation provides an exact way to solve for the ground state electron density, provided we know F_{HK} exactly. The computed electron density can then be used to get the entire ground state configuration of the system being studied. In theory, we have completely solved the many-body Schrödinger equation. Unfortunately, an explicit form for F_{HK} has yet to be found, and much of the cur-

rent research into density functional theory is simply to develop evermore accurate representations of this functional. Over the decades, many approximations have been invented, some more accurate than the others, and some applicable to more complicated systems than others. But it is important to note the power and elegance of the theory explained up to here.

2.3 The Kohn-Sham Equations

Eq. 2.24 provides a unique way to express the energy of the many-electron system as a functional of the electron density. As we have shown, minimizing this functional with respect to the density, and with the usual particle number constraint, produces the ground state energy of the system. All that is needed is an exact representation of the kinetic energy functional, as well as the nonclassical part of V_{ee} due to effects arising from the Pauli Exclusion principle. The model of Thomas and Fermi, assuming a uniform and non-interacting electron gas, produced the kinetic energy functional shown in Eq. 2.21. The non-interacting assumption that lead to this form gives wildly inaccurate results and can hardly be considered for calculations of polyatomic systems with many electrons.

The insight of Kohn and Sham [16] was the decomposition of the kinetic energy functional into two parts: a term representing non-interacting single-particle kinetic energies, and another that represents the remainder [7]. Consider a ground state wave function that is of the form in Eq. 2.8, where ϕ_i orbitals are the N lowest eigenstates of the single-electron Hamiltonian

$$\left[-\frac{\hbar^2}{2m}\nabla^2 + v_s(\mathbf{r}) \right] \phi_i = \epsilon_i \phi_i, \tag{2.28}$$

with $v_s(\mathbf{r})$ the single electron external potential energy. Then decompose $T[n]$ as the sum of a non-interacting energies

$$T_s[n] = \sum_{i=1}^{N} \langle \phi_i | -\frac{\hbar^2}{2m}\nabla^2 | \phi_i \rangle \tag{2.29}$$

and some remainder term $T_c[n]$ which is presumably much smaller than T_s. Then rewrite the total energy functional as

$$E[n] = \int n(\mathbf{r})v(\mathbf{r}) + T_s[n] + J[n] + E_{xc}[n] \tag{2.30}$$

where

$$E_{xc}[n] = T[n] - T_s[n] + V_{ee}[n] - J[n] \tag{2.31}$$

is known as the *exchange-correlation energy*, which contains the difference between the total kinetic energy and the non-interacting kinetic energy (note that $T - T_s$ is assumed to be small), as well as the classical Coulomb and nonclassical electron exchange energies. Upon carrying out the functional derivative with respect to the density, we find that

$$\mu = v_{eff}(\mathbf{r}) + \frac{\delta T_s[n]}{\delta n(\mathbf{r})}, \tag{2.32}$$

where v_{eff} is the effective Kohn-Sham potential

$$v_{eff}(\mathbf{r}) = v(\mathbf{r}) + \int \frac{n(\mathbf{r}_1)}{|\mathbf{r} - \mathbf{r}_1|} d\mathbf{r}_1 + \frac{\delta E_{xc}[n]}{\delta n(\mathbf{r})}. \tag{2.33}$$

With $v_s(\mathbf{r}) = v_{eff}(\mathbf{r})$ and

$$n(\mathbf{r}) = \sum_i^N |\phi_i(\mathbf{r})|^2, \tag{2.34}$$

Eqs. 2.33 and 2.28 are known as the Kohn-Sham equations. They can be solved in the following self-consistent manner to produce the ground state electronic energy. First, start with an initial electron density, $n(\mathbf{r})$, and compute the effective Kohn-Sham potential in Eq. 2.33. That effective potential is then inserted into Eq. 2.28 to produce the N ϕ_i orbitals. Those orbitals are used to compute a new electron density (Eq. 2.34), and the process is started over and only stopped once a desired convergence criterion in the total energy is reached [19].

2.4 Constrained DFT

In the previous sections describing density functional theory from the early developments to the celebrated Kohn-Sham equations, we performed a functional minimization subject to one constraint: that the total number of electrons remains constant throughout. But what if we require the energy functional be minimized subject to multiple constraints, such as ensuring spin or charge distributions remain constant in a molecular system? The work of Qin Wu and Troy Van Voorhis in 2005 [31] does just that. Their work details a method to apply any number of constraints to a given density functional theory calculation, and is known as constrained density functional theory (CDFT).

Consider adding a general constraint to the Kohn-Sham energy functional in Eq. 2.30

$$\int_C n(\mathbf{r})d\mathbf{r} = \int w_C(\mathbf{r})n(\mathbf{r})d\mathbf{r} = N_C, \tag{2.35}$$

where w_C is a weight function that defines the constraint. With this added constraint, we can build up a new energy functional

$$W[n, v_C] = E[n] + v_C\left(\int w_C(\mathbf{r})n(\mathbf{r})d\mathbf{r} - N_C\right) \tag{2.36}$$

where v_C acts as a new Lagrange multiplier for the added general constraint. If we perform a similar minimization to this functional as we did to the functional in the previous section, we find a new set of equations to solve

$$[-\frac{1}{2}\nabla^2 + v_n(\mathbf{r}) + \int \frac{n(\mathbf{r}')}{|\mathbf{r} - \mathbf{r}'|}d\mathbf{r}' + v_{xc}[n](\mathbf{r}) + v_C w_C(\mathbf{r})]\phi_i = \varepsilon_i\phi_i, \tag{2.37}$$

where $v_C w_C$ constitute the *constraint potential*.

These equations are interesting in that for any v_C, the solution orbitals ϕ_i are unique and valid. The task then is to find v_C such that the solutions to the above equations constitute the ground state. The correct multiplier v_C can be found by optimizing the W energy functional with respect to v_C. It is shown in [31] that the extremum found from that optimization is in fact a maximum.

The above discussion leads us to an algorithm for computing the ground state of an electronic system in the presence of added general constraints in the familiar self-consistent manner. First, an initial guess for the orbitals must be supplied to form the Kohn-Sham Hamiltonian. Then, $v_C w_C$ is added to that Hamiltonian with an initial guess for the multiplier v_C. Then we compute the optimal v_C by iteratively solving Eq. 2.37, then computing the optimal v_C as the extremum of W, then inserting that multiplier in the next iteration solution of Eq. 2.37. We've found the correct v_C when the initial general constraint is met. It is known that CDFT calculations suffer convergence problems in practice due to the addition of these extra constraints.

2.4.1 Q-Chem Geometry Optimization for Fe_4

Q-Chem is a quantum chemistry package from Q-Chem Inc. [8] that provides a framework for density functional theory calculations in the presence of added constraints based on the work of Ref. [31]. We have used this package to perform geometry optimization calculations on the Fe_4 (see Sec. 1.3) single-molecule magnet in both the neutral and singly, negatively charged case. All of our calculations used the 6-31G* basis set and the Perdew-Becke-Ernzerhof (PBE) exchange correlation functional [8]. Fig. 2-1 shows an overview of how density functional theory can be used to compute optimal molecular geometries. An initial configuration is provided, such as molecular geometry, general constraints, and an initial solution guess, then we solve the Kohn-Sham equations self-consistently until the desired convergence criteria are met. The specific convergence criteria we consider stipulates that the change in both the overall ground state energy and the intra-molecular forces between iterations is small.

For the neutral molecule geometry optimization calculations, we considered both the case of the molecule exhibiting C_2 and D_3 symmetries, and optimized each one separately. The calculations utilize CDFT by imposing total spin constraints on the iron atoms and their surrounding oxygens. As seen in Fig. 1-4a, each outer iron cation is surrounded by four oxygen anions, while the iron in the center is surrounded by six oxygen anions. The constraints are such that the center iron and its oxygens have a total spin of $-5\mu_B$, while each of the outer iron and corresponding oxygens

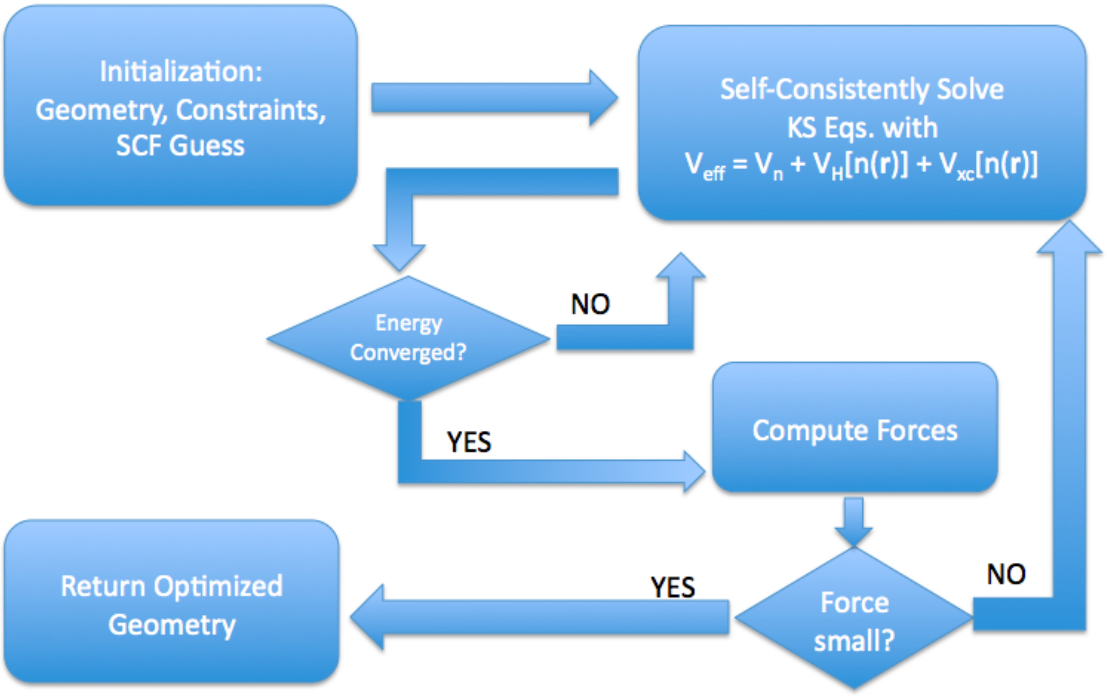

Figure 2-1: Flow chart for geometry optimization using constrained density functional theory.

Molecular Symmetry	Energy (Hartrees)
C_2	-7886.3753291
D_3	-7886.3573305

Table 2.1: Neutral Fe_4 Final Ground State Energy.

Fe_4 Charge Site	Energy (Hartrees)
II	-7886.3918456
III	-7886.3911917
Uniform	-7886.4453419

Table 2.2: Charged Fe_4 Final Ground State Energy.

have a total spin of $5\mu_B$, therefore the total magnetic moment of the neutral Fe_4 is 10 μ_B. The ground state energies for differing symmetry are shown in Table 2.1. For the given convergence criteria, the neutral Fe_4 with C_2 symmetry gives a lower energy than the neutral Fe_4 with D_3 symmetry.

For the charged molecule, the CDFT calculations are inherently more difficult because of two reasons: (1) we must impose a charge constraint in addition to the spin constraints, and (2) there are many different options to add one extra electron to the Fe_4 molecule, which modifies spin constraints as well. In Fig. 2-2, we label each Fe site in the Fe_4 molecule, and consider only the case with C_2 symmetry. We performed calculations for three different charge constraints: the charge constrained (1) to the Fe site II, (2) to the Fe site III (which is equivalent to the IV site for C_2 symmetry), and (3) the charge and spin constrained uniformly across all outer Fe sites (II, III, IV). We disregarded the case of the charge constrained to the Fe I site because the convergence was difficult and the ground state energy would not be lower than the other cases due to stronger Coulomb repulsion. This is due to the fact that it takes more energy to place a charge at the center of the Fe_4 complex do to the interaction of all atoms at the outer sites.

As stated, the presence of a charge introduces a modification to the spin constraints compared to the neutral molecule. When the charge is constrained to the Fe site II or III, the spin constraint for that site must be lowered to 4 μ_B, while in the

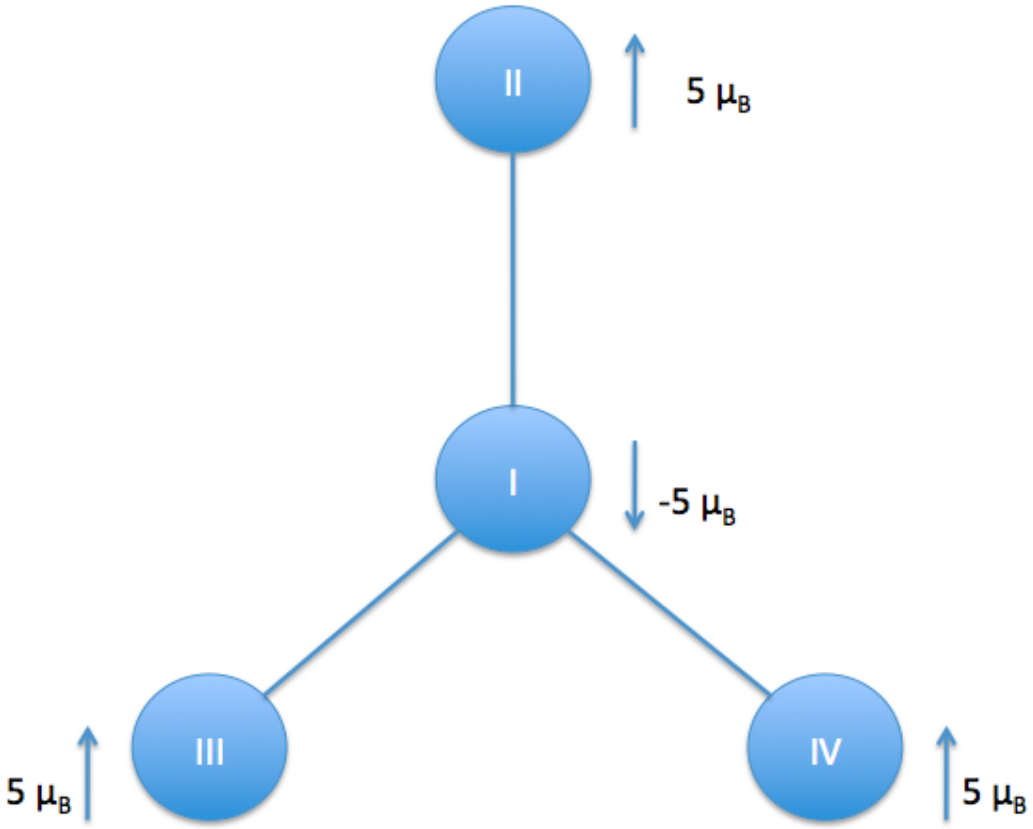

Figure 2-2: Fe_4 iron ion labeling for constrained density functional theory.

uniformly distributed case, the total spin constraint across II, III, and IV must be lowered to 14 μ_B.

The results for these charged cases are shown in Table 2.2. They show that the overall lowest ground state energy occurs for the case of uniformly distributed constraints, i.e. the charge and spin constrained to the II, III, IV.

Chapter 3

Electron Transport Through Single-Molecule Magnets

The features of SMMs discussed in the preceding chapters are fascinating and exciting, but if they are ever to be utilized in any future applications we must be able to manipulate them effectively. In this respect, studies of electron transport through single-molecule magnets are vital, as they will inevitably lead to applications in future spintronics, quantum information, and dense information storage schemes. In this chapter we will elucidate the physics governing the transport of electrons across a single-molecule magnet situated between two electrodes, with a focus on the coupling between electronic and vibrational degrees of freedom. The overall goal will be to arrive at an effective equation of motion for the molecular eigenstate occupation probabilities that can then be used in the calculation of various system observables, such as the SMM junction's current-voltage characteristics. The work derived here will be directly used in the construction of SMMSim, discussed in Ch. 4.

3.1 Transport Model

Fig. 3-1 gives an overall view of the model being considered for SMM electron transport junctions. There are two electrodes, denoted left and right, each with tunneling strength T_L and T_R, and corresponding chemical potentials that can be shifted by

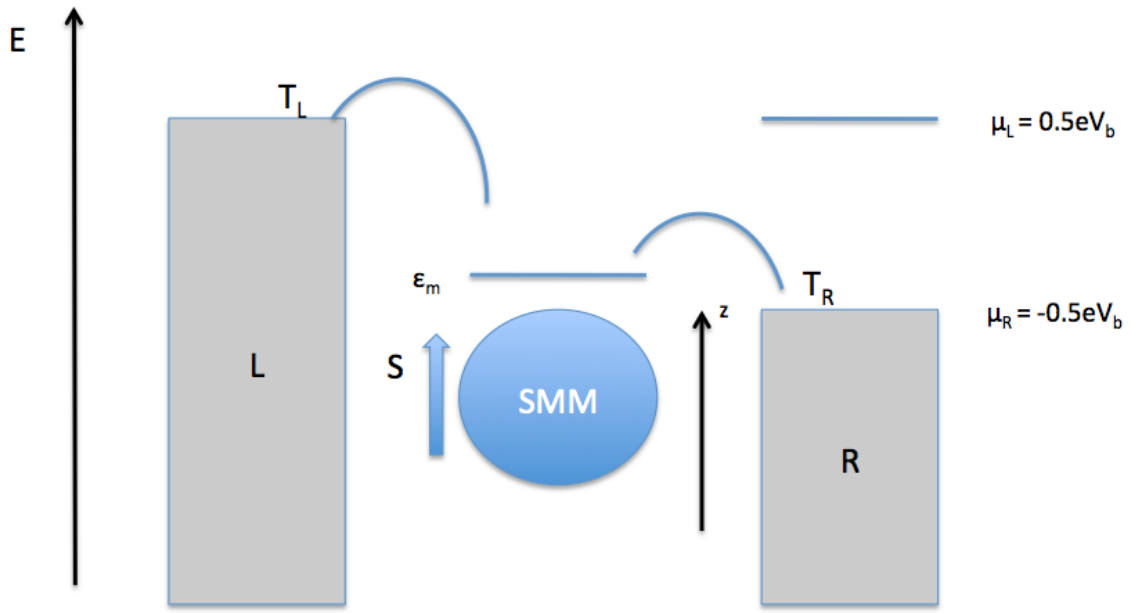

Figure 3-1: Transport model considered in this thesis. It consists of a SMM coupled to two electrodes. Current is induced by a symmetrically applied bias voltage, V_b. Additionally, not shown here is a third terminal which controls a gate voltage V_g that manipulates the energy level ε_m.

an applied bias voltage, V_b, across the junction. We make a number of approximations for this model: (1) we assume weak coupling of the molecule to the electrodes, whereby the overlap between the molecular and electrode wave functions is small; (2) we assume current occurs as sequential tunneling of the electrons through one unoccupied orbital, whose energy is denoted ε_m; (3) we assume a symmetrically applied bias voltage, i.e. as the left electrode chemical potential is increased, the right electrode chemical potential is decrease by an equal amount; and (4) we assume only two charged states of the molecule. Note that not shown in Fig. 3-1 is a third terminal which controls an overall applied gate voltage, V_g, which can be used to change the unoccupied orbital energy ε_m.

This system can be modeled by an effective Hamiltonian that is similar to $\mathcal{H}_{SMM}$ discussed in Sec. 1.2.1 of Ch. 1, but with the addition of terms describing the orbital used by tunneling electrons, the electrodes, and electron tunneling. The Hamiltonian is given by

$$\mathcal{H}_0 = -DS_z^2 + E(S_+^2 + S_-^2) + (\epsilon_m - V_g)\hat{n} + g\mu_B \mathbf{S}\cdot\mathbf{H}, \tag{3.1}$$

where D and E are the uniaxial and transverse magnetic anisotropy constants discussed in Ch. 1, and their values depend on the charge state of the molecule. The number operator for electrons in the orbital ϵ_m is $\hat{n} = \sum_\sigma c_\sigma^\dagger c_\sigma$, where $c_\sigma^\dagger$, c_σ the creation and annihilation operators, respectively, for an electron with spin σ. S_x, S_y, S_z are the x, y, z components of the spin operator, while S_+ and S_- are the spin ladder operators. The last term is the Zeeman energy, with $\mathbf{H}$ being the externally applied magnetic field vector. It should be noted that in the case of Fe_4, the neutral molecule has a total spin of $S = 5$, while the charged molecule has a total spin of $S = 9/2$. This has been confirmed by both DFT and experimental data.

The electrode and tunneling Hamiltonians can be expressed as

$$\mathcal{H}_{el} = \sum_{q=L,R} \sum_{\mathbf{k},\sigma=\uparrow,\downarrow} \varepsilon_{\mathbf{k},\sigma,q} a_{\mathbf{k},\sigma,q}^\dagger a_{\mathbf{k},\sigma,q}, \tag{3.2}$$

and

$$\mathcal{H}_T = \sum_{q=L,R} \sum_{\mathbf{k},\sigma=\uparrow,\downarrow} [T_q a_{\mathbf{k},\sigma,q}^\dagger c_\sigma + T_q^* c_\sigma^\dagger a_{\mathbf{k},\sigma,q}], \tag{3.3}$$

where, $a_{\mathbf{k},\sigma,q}^\dagger$ ($a_{\mathbf{k},\sigma,q}$) create (annihilate) an electron on the q electrode with wave vector $\mathbf{k}$ and spin σ, and $\varepsilon_{\mathbf{k},\sigma,q}$ is the dispersion relation for non-interacting electrons on the q electrode with corresponding wave vector and spin. T_q represents the parameter for tunneling of electrons from the q electrode to the molecule and vice versa.

The sum of these Hamiltonians ($\mathcal{H}_0 + \mathcal{H}_{el} + \mathcal{H}_T$) effectively describes electron transport across a single-molecule magnet in the absence of any molecular vibrations or electron-vibron coupling. To construct the $\mathcal{H}_0$ matrix we use the following basis set:

$$|n = 0, S = 5, M\rangle \tag{3.4}$$

$$\begin{aligned} |n = 1, S \pm \frac{1}{2}, M\rangle = &\pm \sqrt{\frac{S \pm M + \frac{1}{2}}{2S+1}} \left|S, M - \frac{1}{2}\right\rangle |\uparrow\rangle \\ &+ \sqrt{\frac{S \mp M + \frac{1}{2}}{2S+1}} \left|S, M + \frac{1}{2}\right\rangle |\downarrow\rangle . \end{aligned} \tag{3.5}$$

where M is an eigenvalue of S_z, and n is the number of extra electrons in the neutral

molecule. When the molecule is neutral (n=0), our basis states are simply the $2S+1$ spin states. However, when the molecule is charged, we must expand the $|S \pm \frac{1}{2}, M\rangle$ in terms of effective Clebsch-Gordon coefficients [23]. It should be noted that for the case of Fe_4, we ignore the $|S + \frac{1}{2}, M\rangle$ case because it has been shown experimentally that the $|S - \frac{1}{2}, M\rangle$ case is energetically favorable [6].

3.1.1 Transition Rates

Once we have constructed the Hamiltonian matrix with the basis set discussed in the last section, we then compute its energy spectrum and corresponding eigenstates. We are interested in constructing the master equation for the eigenstate occupation probabilities, and so we need to compute the rate of transitions between those states. The formalism for this can be found in standard textbooks, but for this thesis, we follow the formalism summarized in Ref. [18]. The calculation of the transition rates can be done by applying Fermi's golden rule, considering the tunneling Hamiltonian (Eq. 3.3) as a perturbation. We then calculate transition rates from $|i\rangle$ to $|j\rangle$ [18]

$$\gamma^q_{|i\rangle,|j\rangle} = \sum_{\mathbf{k},\sigma} \Big[W_{|i\rangle,|j\rangle} f(\varepsilon^q_{\mathbf{k},\sigma}) + W_{|i\rangle,|j\rangle}[1 - f(\varepsilon^q_{\mathbf{k},\sigma})] \Big], \tag{3.6}$$

where $W_{|i\rangle,|j\rangle} = \frac{2\pi}{\hbar} |\langle j|\mathcal{H}_T|i\rangle|^2 \delta(E_j - E_i)$ is the rate of transitions from initial $|i\rangle$ to the final $|j\rangle$, $f(\varepsilon^q_{\mathbf{k},\sigma})$ is the Fermi-Dirac distribution, $\varepsilon^q_{\mathbf{k},\sigma}$ is the energy of an electron with given $\mathbf{k}$ and σ on the q electrode, and E_i, E_j are the initial and final energies. Since the Fermi-Dirac distribution measures the probability for an electron to exist at the given energy, the first term in Eq. 3.6 describes an electron's transition from the q electrode to the molecule, while the second term describes an electron's transition from the molecule back to the q electrode. By exchanging the sum over $\mathbf{k}$ for an integral and performing the calculation we arrive at a simplified form of Eq. 3.6

$$\gamma^q_{|i\rangle,|j\rangle} = \frac{1}{\hbar} \sum_{\sigma} \Gamma^q_{\sigma} \Big[|C^{\sigma}_{i,j}|^2 f(\epsilon_j - \epsilon_i - \mu_q) + |C^{\sigma}_{j,i}|^2 [1 - f(\epsilon_i - \epsilon_j - \mu_q)] \Big], \tag{3.7}$$

where $|C^{\sigma}_{i,j}|^2 = |\langle j|c^{\dagger}_{\sigma}|i\rangle|^2$, ϵ_i is the molecular energy associated with eigenstate $|i\rangle$, and $\Gamma^q_{\sigma} = 2\pi|T_q|^2 D$ is the orbital level width acquired due to coupling with the q electrode [18]. We assume a constant density of states D near the Fermi level. The matrix elements $|C^{\sigma}_{i,j}|^2$ define certain selection rules for molecular transitions; specifically, they imply that transitions can only occur between uncharged and charged states, and only between states whose M values differ by $\pm\frac{1}{2}$.

The transition rates of Eq. 3.7 depend on the applied bias voltage through the chemical potential of the leads (μ_L, μ_R), and those potentials enter into the Fermi function in Eq. 3.6. Thus, until the chemical potential reaches a certain value, the transitions are suppressed due to the small probability produced by the Fermi functions. This suppression occurs until a valid transition state enters into the *bias window*, or energy range between μ_L and μ_R, the size of which is equal to V_b due to the symmetry of the applied bias (Fig. 3-1). A state is considered a valid transition state if it meets the selection rules discussed previously, that the oxidation state changes by 1 and the change in spin projection M is $\pm 1/2$. This suppression of transitions, and thus the current, is known as the *Coulomb Blockade*, and it can be shifted, or actually removed completely by the application of a gate voltage. As shown before, this gate voltage shifts the energy of the molecular orbital and therefore modifies the computed transition rates.

3.1.2 Master Equation

Using these transition rates $\gamma^q_{|i\rangle,|j\rangle}$, we construct the master equation for the state occupation probabilities as

$$\frac{dP_{|i\rangle}}{dt} = \sum_{q=L,R}\sum_{|j\rangle}(\gamma^q_{|j\rangle,|i\rangle}P_{|j\rangle} - \gamma^q_{|i\rangle,|j\rangle}P_{|i\rangle}), \tag{3.8}$$

where $P_{|i\rangle}$ is the probability for the molecule to be in the eigenstate $|i\rangle$. A quick examination will show that this equation can be expressed in a matrix-vector form as

$$\frac{d}{dt}\mathbf{P} = \tilde{\mathbf{W}}\mathbf{P} \tag{3.9}$$

where

$$\tilde{W}_{i,j} = \begin{cases} \gamma^L_{|j\rangle,|i\rangle} + \gamma^R_{|j\rangle,|i\rangle} & for i \neq j \\ -\sum_{|j\rangle} \gamma^L_{|i\rangle,|j\rangle} - \sum_{|j\rangle} \gamma^R_{|i\rangle,|j\rangle} & for i = j \end{cases} \tag{3.10}$$

i.e. the off-diagonal elements of the matrix $\tilde{\mathbf{W}}$ are transitions from the $|j\rangle$ state to the $|i\rangle$ state, and the diagonal terms are simply the negative sum of their corresponding columns. In this work, we only consider steady state occupation probabilities, i.e., $\frac{d}{dt}\mathbf{P} = 0$, therefore the occupation probabilities governing the current-voltage characteristics of the single-molecule magnet junction can be found by simply computing the null space of $\tilde{\mathbf{W}}$ in Eq 3.9.

The null space of $\tilde{\mathbf{W}}$ is guaranteed to exist because the sum of each its columns is 0, however, it is not guaranteed that the dimension of the null space will be exactly 1. We could have many mathematically valid null space vectors, but not all will be physically valid. This fact, coupled with the knowledge that the transition rate matrix should be highly sparse and diagonally dominant, suggests the use of an iterative solver with the aid of an initial guess solution to speed up convergence and produce physically realistic results. We have chosen the bi-conjugate gradient stabilized method [24] with an initial probability guess that models the Boltzmann distribution

$$P_i = \frac{e^{-\frac{\epsilon_i}{k_B T}}}{\sum_i e^{-\frac{\epsilon_i}{k_B T}}}. \tag{3.11}$$

This method could optionally include the use of a Jacobi preconditioner due to the fact that $\tilde{\mathbf{W}}$ is diagonally dominant [24].

Using the state occupation probabilities, any number of system observables can be computed. The current from the q electrode, for example, is given by

$$I_q = e \sum_{i,j} (n_j - n_i) \gamma^q_{|i\rangle,|j\rangle} P_{|i\rangle}, \tag{3.12}$$

with n_i, n_j the charge state of $|i\rangle$, $|j\rangle$, which in the sequential tunneling regime can

be 0 or 1. The total current is then just

$$I = \frac{I_L - I_R}{2}. \tag{3.13}$$

With these results, the current-voltage characteristics of an SMM transport junction can be constructing by computing the current as a function of the bias voltage and gate voltage. At each bias voltage in a given range we compute the transition rates, solve the master equation by computing the null space of $\tilde{\mathbf{W}}$, and then use that null space vector in the calculation of the current.

3.1.3 Differential Conductance Through Chebyshev Functions

One of the primary use cases for any transport simulation code is to compute the differential conductance over a range of bias and gate voltages. Its importance arises due to the fact that the differential conductance is the primary quantity that experimentalists can measure for these three-terminal devices. The differential conductance at a given bias voltage is defined as the derivative of the total current with respect to the bias voltage, evaluated at that bias voltage. Just using the definition of the derivative, this quantity can be computed as

$$\left.\frac{dI}{dV_b}\right|_{V_b=a} = \lim_{h\to 0} \frac{I(a+h) - I(a)}{h}, \tag{3.14}$$

where a is the point the differential conductance is being computed at, and h is some small step. To implement this, a transport simulation code could pick some small h and evaluate the current at $a + h$ as well as at a and then compute the differential conductance from the results.

This method for computing the differential conductance turns out to be less than ideal. The cost of the computation is large because at each grid point of the calculation, you must compute the current twice, when you have probably already calculated it in another separate total current calculation. The ideal calculation would compute just the total current over this range, and then from that data, produce the overall

derivative at a low cost. In this work, we present a way to do just that by approximating the total current function with Chebyshev polynomials.

The Chebyshev polynomials of degree n are given by

$$T_n(x) = \cos(n \arccos(x)), \tag{3.15}$$

and are orthogonal with weight $(1-x^2)^{-\frac{1}{2}}$ over the range $[-1, 1]$ [20]. It can be shown that an arbitrary function $f(x)$ in the interval $[-1, 1]$ can be approximated by [20]

$$f(x) \approx \left[\sum_{k=0}^{N-1} c_k T_k(x) \right] - \frac{1}{2} c_0. \tag{3.16}$$

with coefficients c_j such that

$$c_j = \frac{2}{N} \sum_{k=0}^{N-1} f(x_k) T_j(x_k), \tag{3.17}$$

for $j = 0, \ldots, N-1$. Furthermore, this approximation can be extended to any arbitrary range by a simple change of variables

$$y = \frac{x - \frac{1}{2}(b+a)}{\frac{1}{2}(b-a)}. \tag{3.18}$$

So approximating a given function f amounts to computing these c_j coefficients through an explicit computation of f and the Chebyshev polynomials. This is a powerful mechanism, in that we basically get the derivative of the function for free. One can show that the Chebyshev approximation of the derivative of f is given by the recursion [20]

$$c'_{j-1} = c'_{j+1} + 2jc_j, \tag{3.19}$$

where c'_j are the Chebyshev coefficients for the derivative approximation, and the recursion starts with $c_N = c_{N-1} = 0$.

With this approximation, we no longer have to explicitly compute the differential conductance. By computing the total current over a given range, and storing it as a

Chebyshev approximated function, we obtain knowledge of the derivative at minimal cost through the recursion relation in Eq. 3.19.

3.2 Incorporating Electron-Vibron Coupling

Electron-vibron coupling has a direct influence on the transport characteristics across single-molecule magnets. Under the sequential tunneling process discussed above, each tunneling electron alters the overall potential felt by the nuclei and therefore induces a shift in the molecule's equilibrium geometry. This leads to a finite probability that the molecule is excited to a vibrational excited state, thus affecting the molecules current-voltage characteristics. To model this quantitatively, we must derive vibrational wave functions and corresponding energies, and use them to compute how it affects transport across the system.

3.2.1 Harmonic Oscillator Approximation

Since the mass of the proton is nearly 2000 times larger than that of the electron, we can approximate the total wave function for a given molecular system as the product of an electron wave function, ψ_e, and a nuclear wave function ψ_n. This is known as the Born approximation, and leaves us with the total wave function $\psi(\mathbf{r}, \mathbf{R}) = \psi_e(\mathbf{r}, \mathbf{R})\psi_n(\mathbf{R})$. The ground state electronic wave function can be computed using the density functional theory approaches discussed in Sec. 2. As for the ground state nuclear wave function, we turn our focus on its explicit computation here, and show that to second order in the nuclear potential, it can be modeled as an uncoupled set of simple harmonic oscillators.

The nuclear Hamiltonian consists of a kinetic part and a component describing the nuclear potential $V_n(\mathbf{R})$, which is given by [24]

$$V_n(\mathbf{R}) = \frac{e^2}{4\pi\epsilon_0}\left[\sum_i Z_i\left(\sum_{i\neq j}\frac{Z_j}{|\mathbf{R}_i - \mathbf{R}_j|} - \sum_j \frac{1}{|\mathbf{r}_j - \mathbf{R}_i|}\right)\right]. \tag{3.20}$$

By defining $\mathbf{Q} = \mathbf{R} - \mathbf{R}_0$ with $\mathbf{R}_0$ the equilibrium geometry, and Taylor expanding

this potential around that equilibrium geometry, one can show that

$$V_n(\mathbf{Q}) = \frac{1}{2}\mathbf{Q}^T\mathbf{K}\mathbf{Q}, \tag{3.21}$$

where $\mathbf{K}$ is the Hessian, a matrix of second derivatives of the potential with respect to the 3N dimensional position (hereafter, N is the number of atoms in the molecule). This expanded potential corresponds to a system of coupled harmonic oscillators, which can be decoupled from diagonalization of the Hessian matrix by solving $(\mathbf{K} - \omega^2\mathbf{M})\mathbf{\Omega} = \mathbf{0}$, where $\mathbf{M}$ is the diagonal matrix whose elements are the masses of the atoms making up the molecule, $\mathbf{\Omega}$ the matrix of normal modes, and ω the normal mode frequencies [25]. The normal-mode coordinates $\mathbf{q}$ are related to the cartesian coordinates $\mathbf{Q}$ by $\mathbf{\Omega}^T\mathbf{q} = \mathbf{Q}$, where $\mathbf{\Omega}^T\mathbf{M}\mathbf{\Omega} = \mathbf{I}$ and $\mathbf{q}$ has units of $\sqrt{kg} \cdot m$. Using $\mathbf{q}$ we arrive at the potential energy corresponding to an uncoupled set of harmonic oscillators

$$V_n(\mathbf{q}) = \mathbf{q}^T\hbar\omega\mathbf{q}. \tag{3.22}$$

With this, we can now express the nuclear Hamiltonian in terms of phonon creation and annihilation operators

$$\mathcal{H}_n = \sum_{i=1}^{\alpha} \hbar\omega_i(d_i^\dagger d_i + \frac{1}{2}). \tag{3.23}$$

The energies and wave functions for a system of α vibrational modes are immediately known from introductory quantum mechanics as [21]

$$\psi_{\mathbf{n}}(\mathbf{q}) = \left(\frac{\det\mathbf{\Gamma}}{\pi^\alpha}\right)^{\frac{1}{4}}\left(\frac{1}{2^{\mathbf{n}}\mathbf{n}!}\right)^{\frac{1}{2}} \exp(-\frac{1}{2}\mathbf{q}^T\mathbf{\Gamma}\mathbf{q})H_{\mathbf{n}}(\mathbf{\Gamma}^{\frac{1}{2}}\mathbf{q}) \tag{3.24}$$

where $\mathbf{\Gamma}$ is the diagonal matrix of reduced vibrational mode frequencies ($\Gamma_{ii} = \frac{\omega_i}{\hbar}$ and $H_{\mathbf{n}}$ are the Hermite polynomials. Notice that $\psi_{\mathbf{n}}$ is indexed by an α dimensional vector that represents the vibrational state; for example, $\mathbf{n} = (0, 1, 0)$ would correspond to a state with three vibrational modes, with the first and third in the ground state, and the second in the first excited state. $2^{\mathbf{n}}$ and $\mathbf{n}!$ correspond to the following products:

$2^{\mathbf{n}} = \prod_{i=1}^{\alpha} 2^{n_i}$ and $\mathbf{n}! = \prod_{i=1}^{\alpha} n_i!$. Additionally, the total energy is the harmonic oscillator energy form

$$E_n = \sum_{i}^{\alpha} \hbar\omega_i(n_i + \frac{1}{2}), \tag{3.25}$$

where n_i is the number of phonons in the i^{th} vibrational mode.

Now that we have an explicit form for the Hamiltonian of a system of molecular vibrational modes, we can modify our model Hamiltonian to include both these modes and the coupling between the tunneling electron and the quanta of those modes.

3.2.2 Modified Model Hamiltonian

With $\mathcal{H}_0$ as before (Eq. 3.1), our new model Hamiltonian with electron-vibron coupling is given by

$$\mathcal{H} = \mathcal{H}_0 + \sum_{i=1}^{\alpha} \left[\lambda_i \hbar\omega_i (d_i^\dagger + d_i)\hat{n} + \hbar\omega_i (d_i^\dagger d_i + \frac{1}{2}) \right]. \tag{3.26}$$

The last term from this Hamiltonian simply describes the energy contribution from the molecule's α vibrational modes, while the second to last term describes the coupling between those modes and the tunneling electron. The strength of this coupling is parameterized by the constant λ_i, and is known as the *electron-vibron coupling strength* for the i^{th} vibrational mode. We will go into more detail on this coupling parameter in the following sections.

It is useful to change to a basis that decouples the electron and phonon degrees of freedom. This can be accomplished using the Lang-Firsov canonical transformation [17], which transforms the Hamiltonian in Eq. 3.26 to $e^S \mathcal{H} e^{-S}$ where $S = \sum_{i=1}^{\alpha} \lambda_i (d_i^\dagger - d_i)\hat{n}$ and the index i is for the i^{th} vibrational mode. By applying this transformation, one can show that the transformed phonon creation (annihilation) operator is $\tilde{d}_i^\dagger = d_i^\dagger - \lambda_i \hat{n}$ ($\tilde{d}_i = d_i - \lambda_i \hat{n}$), the electron creation (annihilation) operator is given by $\tilde{c}_\sigma^\dagger = c_\sigma^\dagger \exp\left[-\sum_{i=1}^{\alpha} \lambda_i (d_i^\dagger - d_i)\right]$ ($\tilde{c}_\sigma = c_\sigma \exp\left[-\sum_{i=1}^{\alpha} \lambda_i (d_i^\dagger - d_i)\right]$), and the occupied orbital energy is renormalized to $\tilde{\epsilon}_m = \epsilon_m - \sum_{i=1}^{\alpha} \lambda_i^2 \hbar\omega_i$. Additionally, this transformation

introduces a shift operator to the tunneling matrix elements

$$T_q \rightarrow T_q e^{-\sum_{i=1}^{\alpha} \lambda_i (d_i^\dagger - d_i)}, \tag{3.27}$$

which directly leads to a low-bias suppression of the current for a large value of λ_i, independent of the applied gate voltage. The physical origin of this shift will be explained in the next section, Sec. 3.2.3.

With this transformation in place, we can express our vibrationally modified molecular Hamiltonian now as

$$\mathcal{H} = \mathcal{H}_0 + \sum_{i=1}^{\alpha} \hbar\omega_i \tilde{d}_i^\dagger \tilde{d}_i, \tag{3.28}$$

where $\tilde{d}_i^\dagger \tilde{d}_i$ is simply a phonon number operator, and the renormalized $\tilde{\epsilon}_m$ is absorbed in the definition of the gate voltage. This Hamiltonian is now diagonal in the phonon degrees of freedom, which will greatly simplify the vibrational analysis in the following sections. To understand how this shift in the tunneling matrix elements manifests itself physically, we turn to the familiar *Franck-Condon Principle* for vibrational excitations.

3.2.3 Franck-Condon Principle

Let us revisit sequential tunneling in the weak coupling regime with the knowledge that our molecular vibrational modes can be approximated as a set of uncoupled harmonic oscillators. Figure 3-2 depicts a simplified view of these potential energies for the neutral and charged cases. We know that when the molecule becomes charged, the overall potential felt by the molecule's nuclei is altered, and this change in potential induces a shift in the equilibrium geometry of the molecule. This shift (shown in Fig. 3-2) in the geometry is directly proportional to the electron-vibron coupling strength λ of a given molecular vibrational mode. Additionally, when this geometric shift occurs, there is a finite probability that the vibrational state of the molecule will become excited. This is a statement of the *Franck-Condon Principle* [25]. The

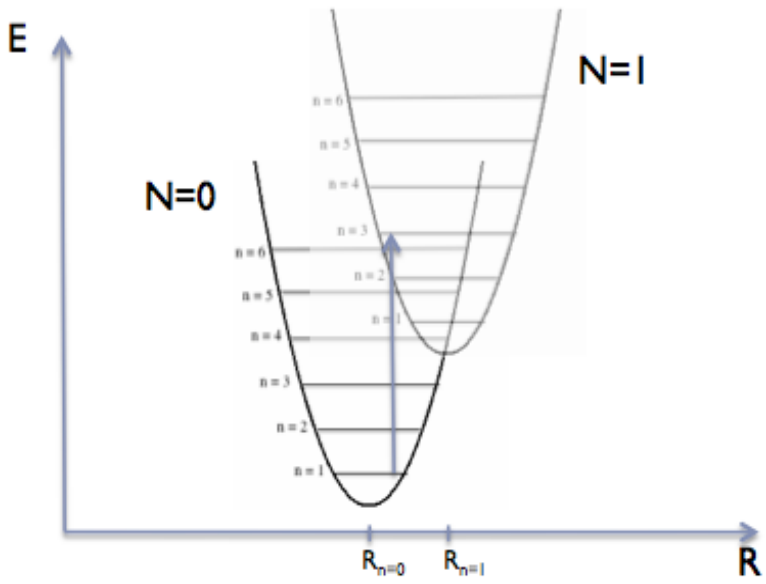

Figure 3-2: Plot depicting tunnel induced change in nuclear geometry as well as induced vibrational excitation. The geometric shift is directly proportional to the strength of the electron-vibron coupling.

probability that this excitation occurs is known as a Franck-Condon factor, and is equal to the square of the overlap between the initial and final vibrational states, which take the form in Eq. 3.24.

Once again utilizing the Born approximation, we can compute the transition rates using Fermi's golden rule, with the tunneling Hamiltonian as the perturbation, in the following manner:

$$|\langle\psi'|\mathcal{H}_T|\psi\rangle|^2 = |\langle\psi'_{\mathbf{n}'}\psi'_{SMM}|\mathcal{H}_T|\psi_{SMM}\psi_{\mathbf{n}}\rangle|^2 = |\langle\psi'_{\mathbf{n}'}|\psi_{\mathbf{n}}\rangle|^2|\langle\psi'_{SMM}|\mathcal{H}_T|\psi_{SMM}\rangle|^2, \tag{3.29}$$

where ψ', ψ are the initial and final states respectively, and the Franck-Condon factor is

$$\mathcal{F}_{\mathbf{n}',\mathbf{n}} = |\langle\psi'_{\mathbf{n}'}|\psi_{\mathbf{n}}\rangle|^2 = |\mathbf{I}_{\mathbf{n}',\mathbf{n}}|^2. \tag{3.30}$$

The overlap integrals $I(\mathbf{n}', \mathbf{n})$ are simply integrals over all space of the product of the initial and final vibrational wave function (Eq. 3.24). The factors in Eq. 3.30 represent the probability of a transition from an initial vibrational state to a final one during the charging and discharging of the molecule in the sequential tunneling regime.

Additionally, these Franck-Condon Factors are multiplied by $|\langle\psi'_{SMM}|\mathcal{H}_T|\psi_{SMM}\rangle|^2$, which is directly proportional the the Fermi golden rule transition rates from Sec. 3.1.1. This implies that the transition rates in the presence of molecular vibrations are just the transitions rates without vibrational coupling multiplied by the appropriate Franck-Condon factor, i.e. $\gamma \to \mathcal{F}_{\mathbf{n}',\mathbf{n}}\gamma$.

These shifted rates were shown to be a consequence of the Lang-Firsov canonical transformation detailed in Sec. 3.2.2. The shift in the tunneling matrix elements from that transformation is a consequence of the shift in the equilibrium geometry of the molecule in the presence of a tunneling charge, which is quantified by the electron-vibron coupling strength, λ.

3.2.4 Computing Franck-Condon Factors

To evaluate the overlap integrals in Eq. 3.30 we must use the vibrational wave functions derived from the harmonic oscillator approximation in Sec. 3.2. Then we have

$$\mathbf{I}(\mathbf{n}',\mathbf{n}) = N\int \psi'_{\mathbf{n}'}(\mathbf{q}')\psi_{\mathbf{n}}(\mathbf{q})d\mathbf{q} = \mathcal{C}\int \exp\left[-\frac{1}{2}(\mathbf{q}'^T\mathbf{\Gamma}'\mathbf{q}'+\mathbf{q}^T\mathbf{\Gamma}\mathbf{q})\right]H_{\mathbf{n}'}(\mathbf{\Gamma}'^{\frac{1}{2}}\mathbf{q}')H_{\mathbf{n}}(\mathbf{\Gamma}^{\frac{1}{2}}\mathbf{q})d\mathbf{q}. \tag{3.31}$$

where N and C are normalization constants. To continue, we need to be able to express the initial normal mode coordinates in terms of the final coordinates. In general, normal modes of a neutral molecule could differ from those of a charged molecule. It is shown in [26] that this corresponds to a Duschinsky transformation

$$\mathbf{q}' = \mathbf{J}\mathbf{q} + \mathbf{k}, \tag{3.32}$$

where $\mathbf{J}$ is the so called Duschinsky rotation matrix, and $\mathbf{k}$ is related to the dimensionless electron-vibron coupling ($\lambda_i = \sqrt{\frac{\omega_i}{2\hbar}}k_i$). The Duschinsky matrix relates the normal modes of a neutral molecule to those of a charged molecule. Upon using this transformation and evaluating the integral, we arrive at an exact expression for the

overlap integral from the vibrational ground state to the vibrational ground state [21],

$$\mathbf{I}(\mathbf{0},\mathbf{0}) = \left(\frac{\sqrt{\det(\mathbf{\Gamma'\Gamma})}}{\det(\mathbf{JS})}\right)^{\frac{1}{2}} \left(\frac{2^{\alpha}}{2^{\mathbf{n}'}\mathbf{n}'!2^{\mathbf{n}}\mathbf{n}!}\right)^{\frac{1}{2}} \exp\left[-\frac{1}{2}\mathbf{k}^T[\mathbf{\Gamma' J S}^{-1}\mathbf{J}^T - \mathbf{1}]\mathbf{\Gamma' k}\right], \quad (3.33)$$

where $\mathbf{S} = \mathbf{J}^T\mathbf{\Gamma' J} + \mathbf{\Gamma}$, and once again, Γ is the diagonal matrix of the normal mode frequencies. The rest of the integrals are found through the recursion relations [21]

$$\begin{aligned}\mathbf{I}(0,\cdots,n'_m,\cdots,n'_\alpha;0,\cdots,0,n_m,\cdots,n_\alpha) = \frac{1}{(2n'_m)^{\frac{1}{2}}}\Bigg[b_m I(n'_m-1) \\ +(2(n'_m-1))^{\frac{1}{2}}A_{mm}I(n'_m-2) + \sum_{k=m+1}^{\alpha}\left(\frac{n'_k}{2}\right)^{\frac{1}{2}}(A_{mk}+A_{km})I(n'_m-1,n'_k-1) \\ + \sum_{k=m}^{\alpha}\left(\frac{n_k}{2}\right)^{\frac{1}{2}}E_{km}I(n'_m-1;n_k-1)\Bigg]\end{aligned} \quad (3.34)$$

for $n'_m > 0$ and

$$\begin{aligned}\mathbf{I}(0,\cdots,n'_{m+1},\cdots,n'_\alpha;0,\cdots,0,n_m,\cdots,n_\alpha) = \frac{1}{(2n_m)^{\frac{1}{2}}}\Bigg[d_m I(n_m-1) \\ +(2(n_m-1))^{\frac{1}{2}}C_{mm}I(n_m-2) + \sum_{k=m+1}^{\alpha}\left(\frac{n_k}{2}\right)^{\frac{1}{2}}(C_{mk}+C_{km})I(n_m-1,n_k-1) \\ + \sum_{k=m+1}^{\alpha}\left(\frac{n'_k}{2}\right)^{\frac{1}{2}}E_{mk}I(n'_k-1;n_m-1)\Bigg]\end{aligned} \quad (3.35)$$

for $n_m > 0$, where for shorthand we have

$$I(n'_m-1) = I(0,\cdots,n'_m-1,n'_{m+1},\cdots,n'_\alpha;0,\cdots,0,n_m,\cdots,n_\alpha), \quad (3.36)$$

$$I(n'_k-1;n_l-1) = I(0,\cdots,0,n'_m,\cdots,n'_k-1,\cdots,n'_\alpha;0,\cdots,0,n_m,\cdots,n_l-1,\cdots,n_\alpha), \quad (3.37)$$

$$\mathbf{A} = 2\mathbf{\Gamma'}^{\frac{1}{2}}\mathbf{J S}^{-1}\mathbf{J}^T\mathbf{\Gamma'}^{\frac{1}{2}} - \mathbf{1}, \quad (3.38)$$

$$\mathbf{b} = 2\mathbf{\Gamma'}^{\frac{1}{2}}[\mathbf{1} - \mathbf{J S}^{-1}\mathbf{J}^T\mathbf{\Gamma'}]\mathbf{k}, \quad (3.39)$$

$$\mathbf{C} = 2\mathbf{\Gamma}^{\frac{1}{2}}\mathbf{S}^{-1}\mathbf{\Gamma}^{\frac{1}{2}} - \mathbf{1}, \quad (3.40)$$

$$\mathbf{d} = -2\boldsymbol{\Gamma}^{\frac{1}{2}}\mathbf{S}^{-1}\mathbf{J}^{T}\boldsymbol{\Gamma}'\mathbf{k} \tag{3.41}$$

$$\mathbf{E} = 4\boldsymbol{\Gamma}^{\frac{1}{2}}\mathbf{S}^{-1}\mathbf{J}^{T}\boldsymbol{\Gamma}'^{\frac{1}{2}}. \tag{3.42}$$

Using these relations, one can calculate the probability of a vibrational transition between any two states. For our calculations we take the case where the Duschinsky mixing matrix is set to unity, $\mathbf{J} = \mathbf{I}$, and the initial and final frequencies are the same, $\boldsymbol{\Gamma}' = \boldsymbol{\Gamma}$. This implies that $\mathbf{A}$, $\mathbf{C} = \mathbf{0}$, $\mathbf{E} = 2\mathbf{I}$, $\mathbf{b} = \sqrt{2}\lambda$, and $\mathbf{d} = \sqrt{2}\lambda$.

Note that these recursion relations are unwieldy, and the total number of possible Franck-Condon factors grows like

$$\binom{\alpha + n_q}{n_q}, \tag{3.43}$$

where n_q is the total number of possible vibrational quanta to consider. Ch. 4 will detail an efficient computational method for computing these overlap integrals for any number of modes and quanta.

3.2.5 Franck-Condon Blockade

Notice in Eq. 3.33 that the overlap between the vibrational wave functions is proportional to $\exp(-\mathbf{k}^{T}\mathbf{k})$, where, as stated previously, $\mathbf{k}$ is a measure of the electron-vibron coupling strength λ. This implies that as the strength of the coupling increases, the magnitude of the probabilities for vibrational transitions goes down. And since the transition rates are multiplied by these Franck-Condon probabilities in the presence of vibrational coupling, the transitions between the eigenstates of our model Hamiltonian are exponentially suppressed as the strength of the electron-vibron coupling increases. Therefore, it takes more energy to achieve these state transitions, i.e., a higher applied bias voltage. This low bias suppression of the transitions, and thus the current, is known as the *Franck-Condon Blockade* [15], and it differentiates itself from the Coulomb Blockade in that it cannot be lifted or altered by an applied gate voltage. This is the interesting physics that we expect to see when we incorporate vibrational coupling into our transport simulations.

3.2.6 Electron-Vibron Coupling

The strength of the electron-vibron coupling can be explicitly computed using the following equation

$$\lambda = \sqrt{\frac{\omega}{2\hbar}}\mathbf{\Omega}^T\mathbf{M}(\mathbf{R}_{n=1} - \mathbf{R}_{n=0}). \tag{3.44}$$

This gives a vector of electron-vibron couplings for each of the $3N - 6$ vibrational modes of the molecule. Here, $\mathbf{\Omega}$ is the matrix of vibrational normal mode coordinates, $\mathbf{M}$ is the diagonal matrix of atomic masses, and $\mathbf{R}_{n=1}$, $\mathbf{R}_{n=0}$ are the equilibrium geometries for the charged and neutral cases, respectively. These values can be garnered through density functional theory calculations, discussed in Ch. 2. Most density functional theory software packages provide vibrational mode calculations, as well as routines for molecular geometry optimizations. Our results for these calculations will be detailed in Ch. 5.

Chapter 4

SMMSim: Single-Molecule Magnet Simulator

SMMSim is a simulator for electron transport across single-molecule magnets under the weak coupling and sequential tunneling approximations. It provides a mechanism for computing the current-voltage characteristics of a single-molecule magnet with, or without, the addition of molecular vibrational modes. It is an object-oriented C++ application, developed with a strong focus on modularity, abstraction, and future scalability. Its development and implementation has employed a number of software-engineering best practices, such as model driven development [2] with the Unified Modeling Language (UML) [14], and test-driven development (TDD) [13].

In keeping with this object-oriented and modular philosophy, the functionality of SMMSim has been decomposed into various stand-alone classes or libraries:

- *FranckCondonTree* - This class is used to compute the Franck-Condon factors discussed in Sec. 3.2.3 of Ch. 3. It utilizes the state-tree algorithm described in [22].

- *Hilbert* - This library defines the classes necessary to construct elements of a Hilbert space, and is used by SMMSim to construct model Hamiltonians. It provides a defining interface for these operators, as well as an interface that describes states that may be operated upon by those operators.

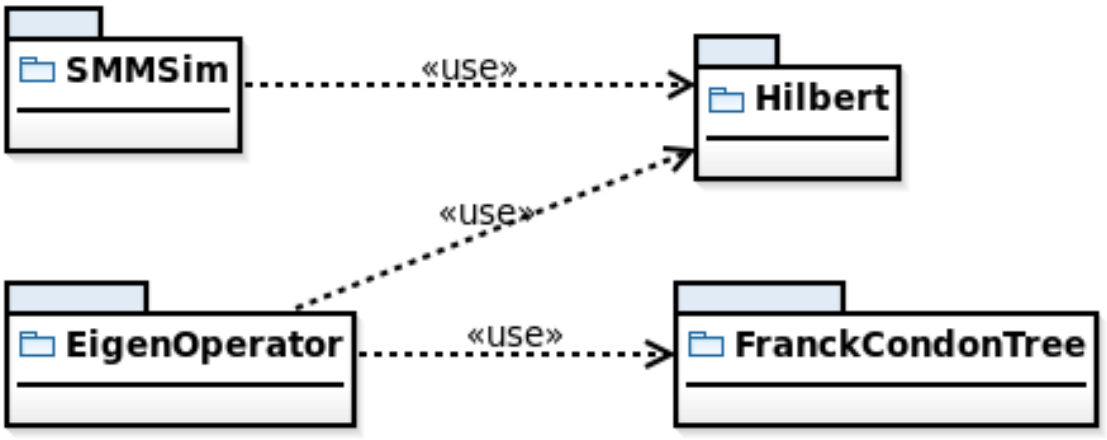

Figure 4-1: SMMSim component diagram, depicting SMMSim's relationship to the Hilbert, EigenOperator, and FranckCondonTree components.

- *EigenOperator* - This library provides a concrete realization of Hilbert's operator interface that utilizes the popular C++ linear algebra package Eigen [11].

As seen in Fig. 4-1, SMMSim brings together all these component's functionality and provides methods for computing the current-voltage characteristics of a user-described single-molecule magnet coupled to two electrodes. The remainder of this Chapter will elaborate on the specific details of these components, including their overall structure and function.

4.1 FranckCondonTree

The computation of Franck-Condon factors using the recursion relations defined in Sec. 3.2.3 of Ch. 3 can be quite tedious, as the total number of possible vibrational states for α modes and n_q excitations is $\binom{\alpha+n_q}{n_q}$. The fact that the factors are indexed by the initial and final vibrational states indicates that they may form some type of multi-dimensional array, but how can we structure that array to optimize overall computational efficiency? It is clear that we will need to develop some mapping between a given state vector $\mathbf{n} = (n_1, n_2, \ldots, n_\alpha)$ and some integer index p, call it $\mathcal{M} : \mathbf{n} \rightarrow p$, that can be used to define $\binom{\alpha+n_q}{n_q}$ x $\binom{\alpha+n_q}{n_q}$ matrix of Franck-Condon factors, $\mathcal{F}_{p',p}$, which can be efficiently modeled and handled by a computer. The

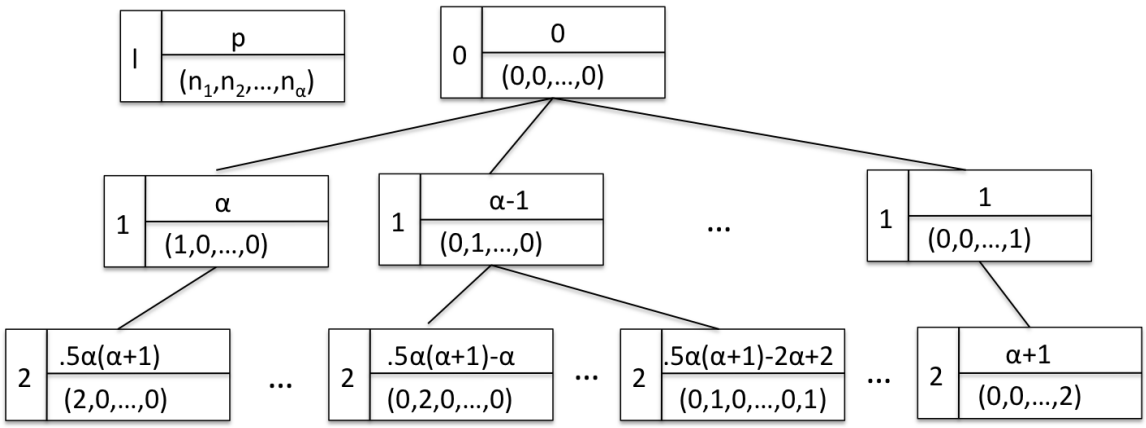

Figure 4-2: Graphical representation of the mapping $\mathcal{M}$ taking vibrational states to integer indices. Each node details the corresponding position and level in the state tree. This structure is used to create a matrix of Franck-Condon factors.

method we will detail now is based on constructing $\mathcal{M}$ in a way that creates a tree of vibrational states, and is taken from [22].

Fig. 4-2 shows this overall tree structure mapping. Each node in the tree represents a vibrational state with a corresponding position in the tree p, which is the mapped index discussed above. Each node also shows its overall tree level number l, defined by $l = \sum_{i=1}^{\alpha} n_i$, which describes the level of the tree on which a given vibrational state resides. Clearly, as we walk the tree and increment the p index, we get a new vibrational state. For each level, there are S possible permutations of vibrational states, which is given by

$$S(\alpha, l) = \binom{\alpha + l - 1}{l}. \tag{4.1}$$

There are therefore $N = \sum_{i=0}^{l} S(\alpha, i)$ total nodes, i.e. N total vibrational states. Additionally, each node conveys a branch number b, which details on which branch of the parent node the given node exists, and conveys the index of the first nonzero entry in the vibrational state vector.

With this tree structure in place and the position, level, and branch values just described, we are in a position to design an algorithm to compute all Franck-Condon factors using the recursion relations in Sec. 3.2.3 of Ch. 3. To do this, we have developed *FranckCondonTree*, shown in Fig. 4-3, which contains a matrix indexed by the

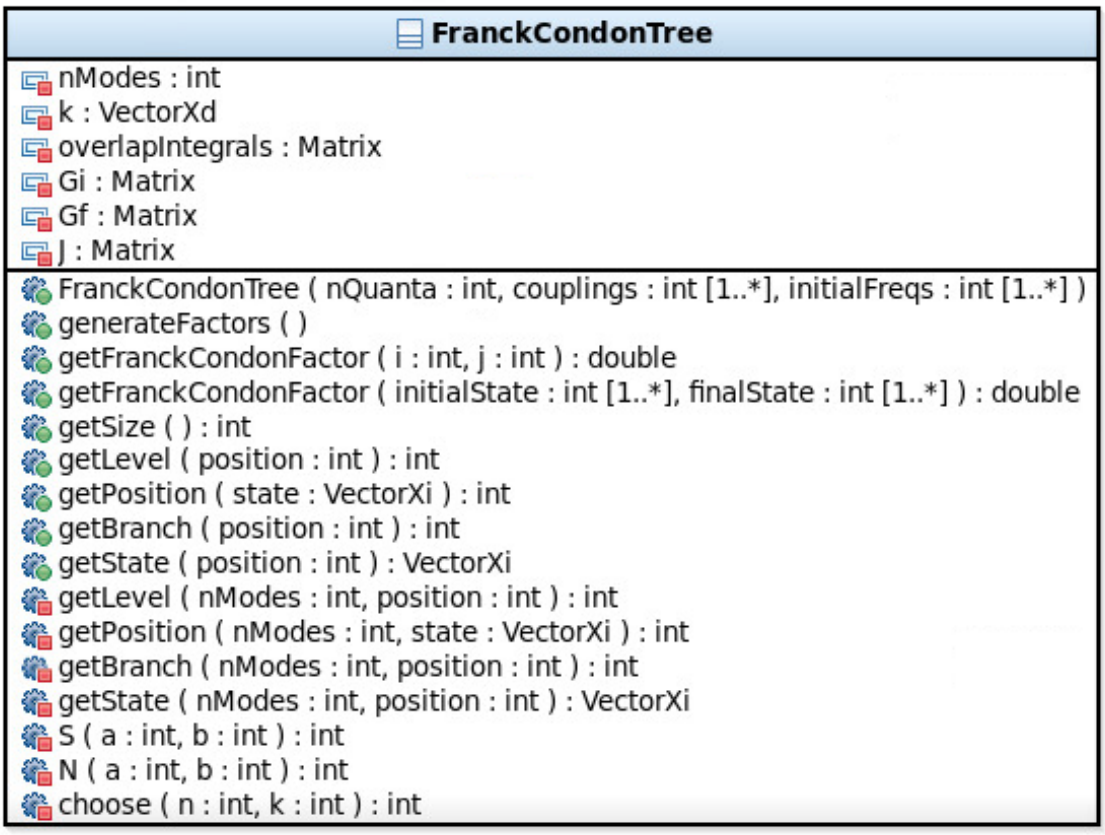

Figure 4-3: FranckCondonTree object model, showing internal data structures for storing the couplings and frequencies, and the computed overlap integrals.

initial and final vibrational state positions, p' and p, that stores the overlap integrals computed from the recursion relations. Before we can compute those overlaps, we need algorithms to get the level, position, and branch of a given vibrational state, each conveniently represented as a method of the FranckCondonTree class: *getLevel*, *getPosition*, *getBranch*, *getState*. For brevity, these algorithms will not be detailed here, but can be found in their entirety in [22].

To perform calculations with Franck-Condon factors, one simply instantiates a FranckCondonTree with the total number of desired vibrational excitations to consider, the electron-vibron coupling constants, and the phonon frequencies, and then invokes the *generateFactors* method to compute all the overlap integrals. The corresponding squares of those overlaps are accessed through the *getFranckCondonFactor* methods, which can take the position indices, or the actual initial and final vibrational

states.

4.2 Hilbert

Hilbert is a library that provides the functionality necessary to describe elements in a Hilbert space. It contains a number of abstractions that users can utilize to create quantum states, and operators that act on those states. Additionally, Hilbert provides a container object for these state objects, which can be used to model a basis set for the space. Operators can then be constructed with a given basis set and use the states in that set to compute the elements of the operator's internal matrix representation.

The combined effort of these abstractions and the C++ operator overloading mechanism provide a powerful mechanism for the construction of model Hamiltonians. Users simply define a basis set and use it to create any quantum operator, such as an electron creation operator or the z-component of a molecule's spin operator. These constituent operators can then be used in basic arithmetic expressions to construct an overall Hamiltonian.

4.2.1 State and BasisSet

The *State* class abstracts the basis states defined in Eqs. 3.4, 3.5 of Sec. 3.1 in Ch. 3, and in doing so, encapsulates the charge, spin, and vibrational state of a given single-molecule magnet coupled to two electrodes. It provides methods that allow users to create electrons or phonons on the molecule, measure and raise the molecule's spin projection quantum number, and compute the inner product with other States. State adheres to the familiar Composite design pattern [10] so that the state itself can be composed of other states. This tree pattern allows Hilbert to model quantum states that are superpositions of simpler states, such as the expanded charged states in Eq. 3.5. In accordance with the Composite pattern, State is accompanied by a *CompositeState* class that is itself a generalization of State. The overall structure of this pattern can be seen in Fig. 4-4, and shows that CompositeState contains a set of States and provides tailored implementations of the crucial State methods.

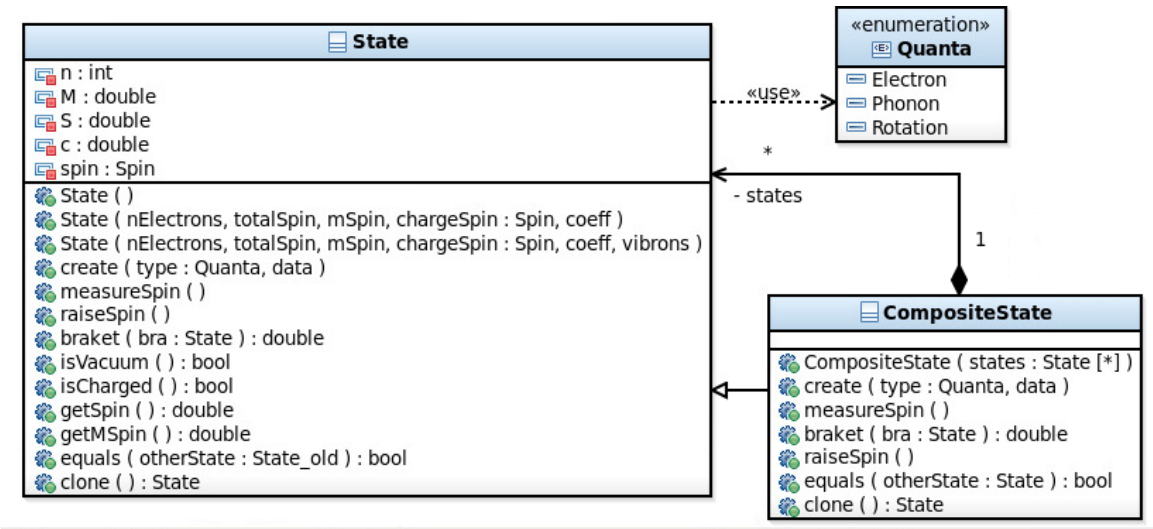

Figure 4-4: The State object model, showing its overall tree structure with CompositeState representing a node in that tree with children States.

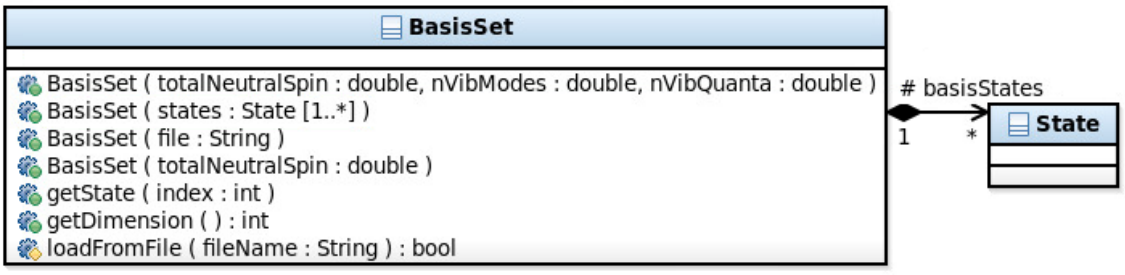

Figure 4-5: BasisSet object model, exhibiting its composition of State objects.

Sets of these State instances can be used to model or construct a *BasisSet*. This class encapsulates the data necessary to describe a basis for the Hilbert space being considered in the construction of various operators and model Hamiltonians. It wraps a list of States, which can be created either externally and injected in the creation of a BasisSet, or internally through the use of BasisSet's default constructors. The default constructors for this class construct the basis described by Eqs. 3.4, 3.5 of Sec. 3.1 in Ch. 3, and BasisSet provides methods for users to access and modify those States.

4.2.2 Operator

The *Operator* abstract class defines the main abstraction provided by Hilbert, and encapsulates the functionality necessary to create an operator in a Hilbert space defined by an injected BasisSet. The basis set data encapsulated by this injected BasisSet is then used by subclasses of this class in the concrete construction of the Operator's internal matrix representation. All subclasses must define and keep track of this matrix representation, and provide functionality to compute the Operator's eigenvalues, eigenvectors, null space, and various system observables. Users do not concern themselves with the internal representation or construction of a given Operator; they only care that the Operator can give them this information. This keeps SMMSim, the primary client of the Hilbert library, agnostic to the way model Hamiltonians are created and stored, and endows SMMSim with the flexibility to run with dense or sparse matrix storage schemes, as well as sequential or massively parallel matrix multiplication paradigms.

Fig. 4-6 shows the overall structure of the Operator, and one can immediately notice the flexibility of this class to keep users agnostic about the internal structure of the Operator matrix. *EigenOperator* realizes the Operator interface and provides an internal matrix representation based on the Eigen C++ linear algebra package [11]. Other subclasses can just as easily be defined, such as an Operator based on the Portable, Extensible Toolkit for Scientific Computing (PETSC) [3], which utilizes the Message Passing Interface (MPI) to model large, sparse matrix representations in an

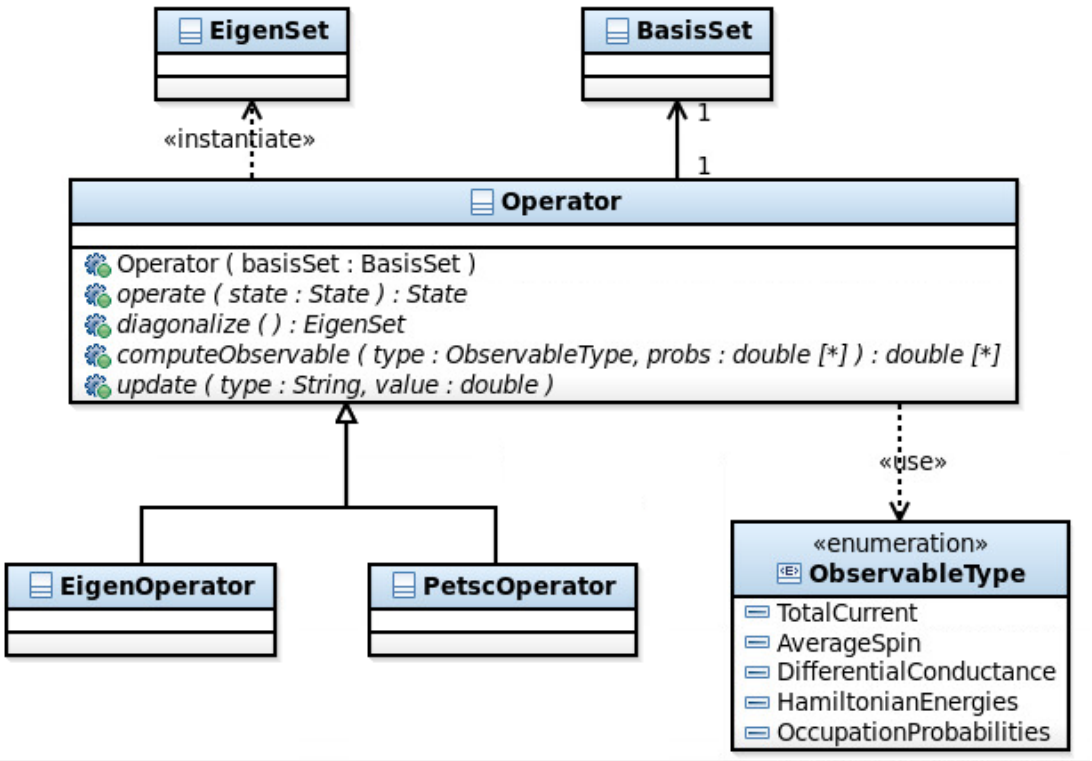

Figure 4-6: Operator interface object model, showing various realizations and utility classes necessary to achieve its stated functionality.

efficient and parallel manner.

Primary amongst the methods Operator provides is the *operate* method. This protected method is only visible to subclasses of Operator, and can be used to perform the Operator's specific function on a given State. For example, this method may be implemented by an electron creation Operator subclass to create an electron on the provided State. If successful, this method would return the resultant oxidized State, while if unsuccessful, would return the vacuum State. It should be noted that this method is intended to alter the incoming State, so users should pass a clone if they require the State instance to be used again. This behavior is intended to mimic the actual method of measuring or operating on a ket vector, which produces an eigenvector of the Operator.

Operator subclasses can also provide tailored implementations of the *diagonalize*, *computeNullSpace*, and *computeObservable* methods that utilize their particular matrix representation. The *diagonalize* method should compute the eigenvalues and eigenvectors of the matrix and return them as an *EigenSet*, a utility class that takes the eigenvalues and eigenvectors as input, and places them in a map that associates the eigenvalue to its corresponding eigenvector. It also defines a particular ordering, so that users can utilize this information in a uniform manner.

The *computeNullSpace* method should be implemented by realizations of the Operator interface to compute the solution vector of the matrix equation $\mathbf{Ax} = \mathbf{0}$. Since the dimension of the null space may be greater than one, it is left up to subclasses to decide what constitutes a physically realistic null space vector. This method is used by SMMSim to compute the eigenstate occupation probabilities described in Sec. 3.1.2 of Ch. 3. Some iterative solution methods require an initial solution guess to achieve convergence in an efficient manner, so this method gives users the option of starting the calculation with this initial guess.

Finally, the *computeObservable* method can be used by users to calculate various transport or molecular observables. Observables such as the total current across the molecule, the molecule's discrete energy spectrum, or the current eigenstate occupation probabilities are all examples of observables users may request.

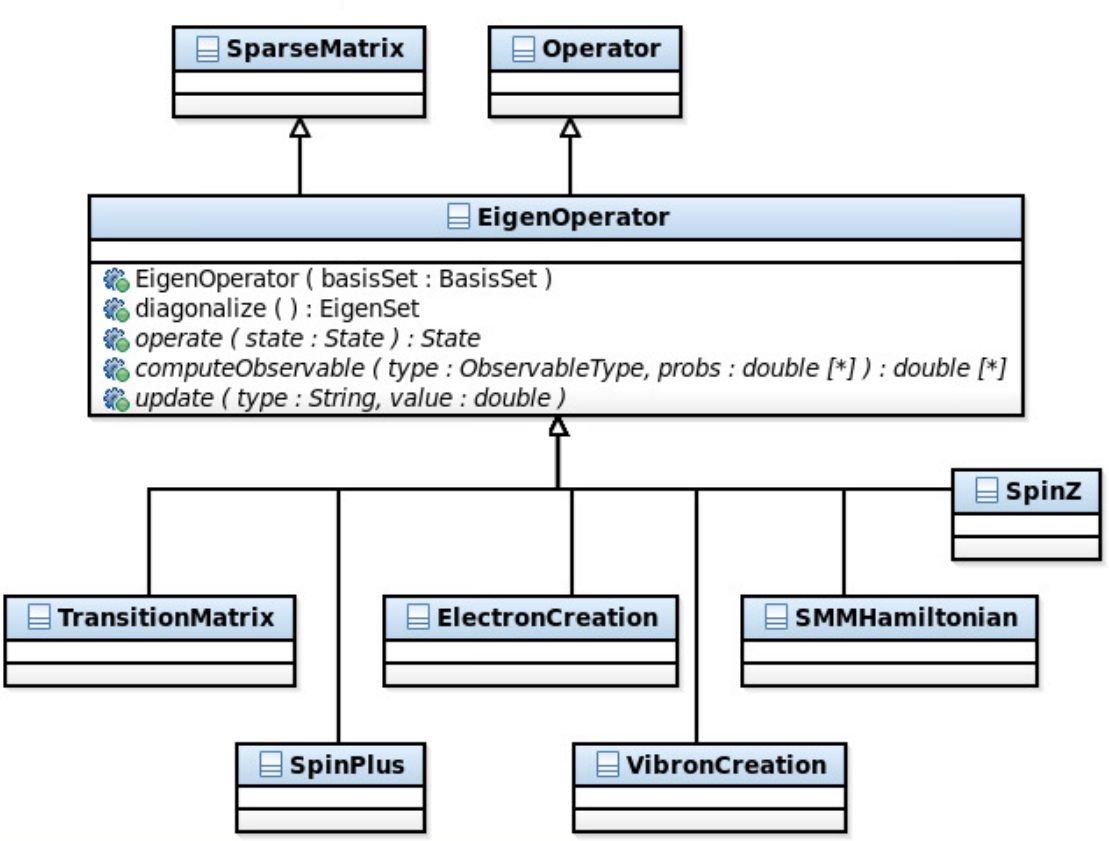

Figure 4-7: EigenOperator object model, showing its inheritance structure and various operator subclasses.

Hidden in the Operator interface is another well-known software design pattern. The Observer design pattern [10] is realized here with the *update* method (see Fig. 4-6). Operators can be registered with valid data subjects to be notified of any changes in subject data state. The *SMMInput* class, for example, is a valid subject Operators may observe, and any changes to the user input data during runtime will trigger a call to the Operator's update method. This allows users to compute system observables over a range of values, such as the total current as a function of a variable applied bias voltage.

4.3 EigenOperator

EigenOperator is SMMSim's default Operator subclass that uses the Eigen C++ linear algebra package [11] for its internal matrix representation. Since most operators

in the Hilbert space defined by the BasisSet in Eqs. 3.4 and 3.5 will be sparse, EigenOperator additionally subclasses Eigen's *SparseMatrix* class, which offers a variant of the compressed column storage scheme by encapsulating arrays that only store the EigenOperator's nonzero values, row and column indices, and the number of nonzeros in each column [11]. This provides an efficient and versatile method for matrix storage, manipulation, and multiplication that leads to an increase in overall compute speed.

The EigenOperator inheritance structure, shown in Fig. 4-7, provides a truly powerful augmentation of the Operator abstraction. In addition to the sparse storage scheme, EigenOperator gets overloaded arithmetic operators for free. Through the C++ operator overloading mechanism, SparseMatrix, and thus EigenOperator, defines a set of arithmetic operations that allow these matrices to be constructed, multiplied, and added together in an extremely intuitive manner, and lets users create model Hamiltonians or other composite operators with ease.

The following code snippet shows how a simple Hamiltonian can be constructed with EigenOperators:

```
// Create orbital energy, magnetic anisotropy,
// and strength of z-component of magnetic field
double energy = 1.0, Hz = 1.0, D = 1.0, spin = 5.0;
// Create the Hilbert space basis set
BasisSet basis(spin);
// Create electron creation and number operators
ElectronCreation cDagUp(basis, Spin::UP), cDagDown(basis, Spin::DOWN);
EigenOperator nUp = cDagUp * cDagUp.transpose(), nDown = cDagDown *
    cDagDown.transpose();
// Get total number operator
EigenOperator n = nUp + nDown;
// Create the z-component of molecule's total spin operator
SpinZ Sz(basis);
// Create simple Hamiltonian with one level for sequential tunneling
```

```
EigenOperator H = -D * Sz * Sz + energy * n - Hz * Sz;
// Get eigenvalues and eigenvectors
EigenSet eigenSet = H.diagonalize();
```

ElectronCreation, a subclass of EigenOperator that models the $c_\sigma^\dagger$ operator, can be constructed from a given BasisSet instance and used to construct the familiar number operator, $\hat{n}$. Similarly, an S_z EigenOperator subclass can be created, and both used in the construction of a sparse Hamiltonian. Finally, through the interface defined by Operator, users can compute the eigenvalues and eigenvectors in a simple, elegant fashion by just invoking the *diagonalize* method on the constructed Hamiltonian EigenOperator.

The EigenOperator package provides a number of subclasses, but primary amongst these are the SMMHamiltonian and TransitionMatrix subclasses. These objects create themselves using a variety of the other EigenOperator subclasses shown in Fig. 4-7. We will therefore elucidate the details of these objects in the following subsections.

4.3.1 SMMHamiltonian

SMMHamiltonian, shown in Fig. 4-8, subclasses EigenOperator and provides construction routines that build up the model Hamiltonian described in Eq. 3.26 in Ch. 3. As a further subclass of SparseMatrix, it encapsulates a sparse matrix storage scheme and can be used in any arithmetic operations. It encapsulates the data necessary to describe a single-molecule magnet's magnetic anisotropy, transport energy level, applied gate voltage and external magnetic field, and the vibrational coupling strengths and frequencies. Using this data, it constructs itself in a manner similar to the code snippet displayed above. It provides an implementation of the *diagonalize* method that uses Eigen's *SelfAdjointEigenSolver* class to compute its eigenvalues and eigenvectors, and uses that data in the construction of a valid EigenSet object. It's *computeObservable* method allows users to get the SMMHamiltonian's energy spectrum, while its *update* method allows the computation of that spectrum over a range

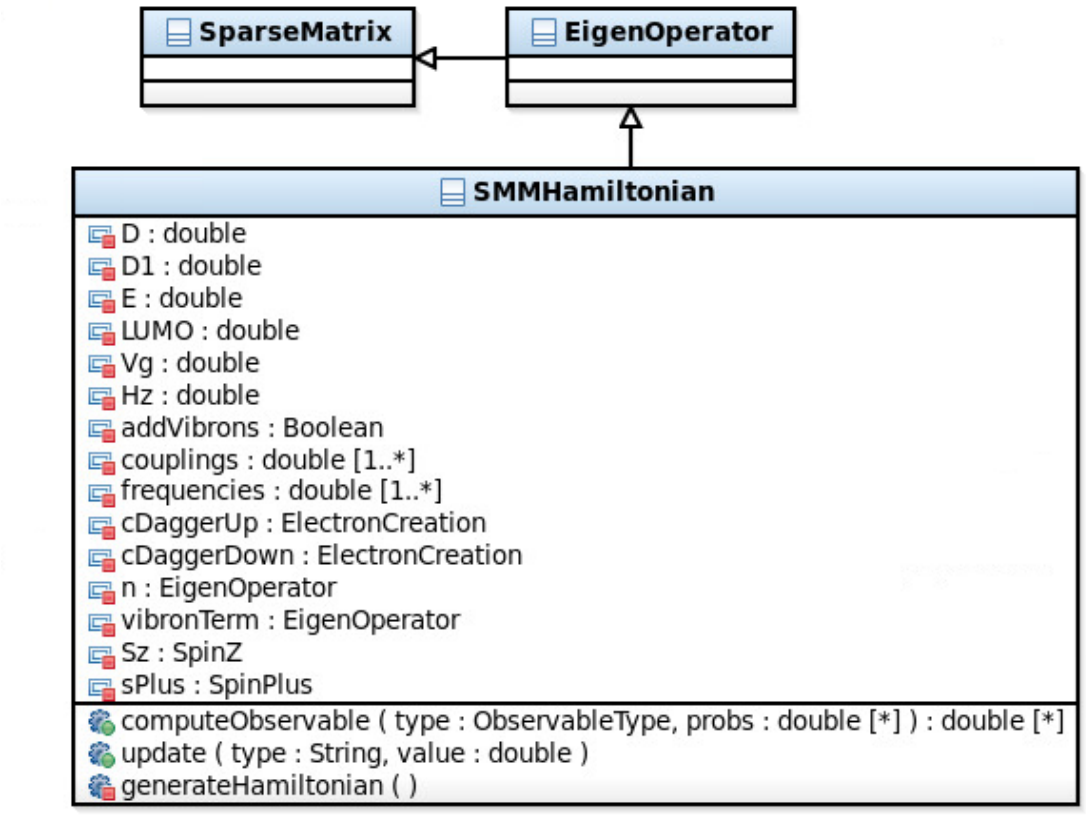

Figure 4-8: SMMHamiltonian object model, showing its inheritance structure and the data it encapsulates to describe the model Hamiltonian of a single-molecule magnet coupled to two electrodes.

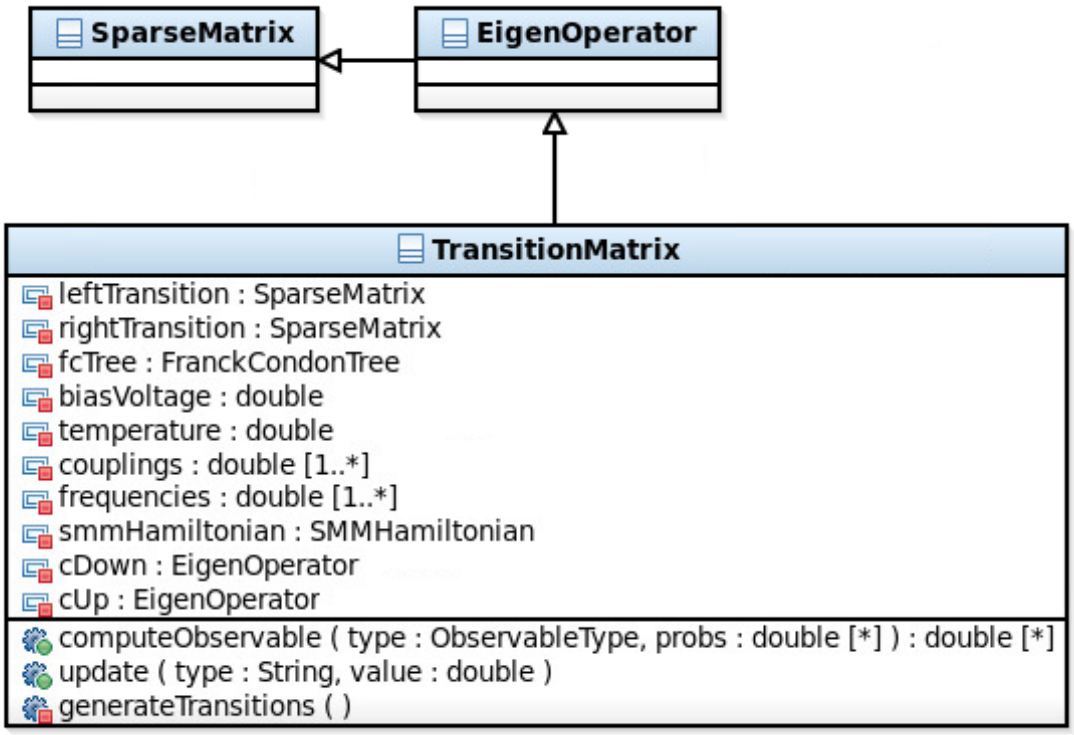

Figure 4-9: TransitionMatrix object model.

of gate voltages or external magnetic fields.

4.3.2 TransitionMatrix

TransitionMatrix is a subclass of EigenOperator that encapsulates the matrix of transition rates found in Eq. 3.9 of Ch. 3. Even though this matrix of transitions is not an actual quantum operator, a conscious design decision was made to have it subclass EigenOperator to reuse as much code base as possible. Specifically, TransitionMatrix subclasses EigenOperator to take advantage of its internal sparse matrix representation. The transition rates themselves are elements of EigenOperator's matrix representation, and are constructed from knowledge about the SMMHamiltonian's EigenSet, the bias voltage, and the vibrational couplings and frequencies. That vibrational data is used to construct an instance of the FranckCondonTree, which is then used in the calculation of the vibrationally-suppressed transition rates.

Its *computeObservable* method provides an implementation that allows users to

compute the total current, differential conductance, and average total spin, all over a range of applied bias voltages. These observables are computed by calculating the null space of the TransitionMatrix's, which represents the vector of eigenstate occupation probabilities. TransitionMatrix uses the bi-conjugate gradient stabilized method (BiCGSTAB) [28] to compute its null space, which is an iterative solver that can incorporate both an initial guess solution as well as a preconditioner to improve its convergence. The matrix of transitions benefits from this solver since it is sufficiently sparse, and can be initialized from a physically realistic Boltzmann distribution for the occupation probabilities. A Jacobi preconditioner can improve the overall efficiency of this method for the TransitionMatrix, since by definition the matrix is diagonally dominant.

4.4 SMMSim

SMMSim ties all the previously discussed components together into one framework, and in doing so, enables users to compute a wide-range of observables for a user-defined SMM transport system. Fig. 4-10 shows SMMSim's overall structure, and exhibits a strong dependence on the well-known *Factory* design pattern [10]. SMMSim makes use of factories for constructing Operators and *SMMInput* instances, which abstract the user-defined input data necessary for a given simulation of an SMM transport system. This factory dependence ensures that SMMSim remains Operator and SMMInput agnostic. It does not care what the underlying Operator matrix structure is, only that they can be created and queried for eigenvalues, eigenvectors, and other operator observables. In a similar manner, the factory object for SMMInput instances lets SMMSim utilize many different input file types. For example, the default SMMInput subclass reads in the NEAMS Integrated Computational Environment (NiCE - *niceproject.sourceforge.net*) defined Painfully Simple Form file type, so SMMSim can utilize all *.psf file types for user input. Others can be created, such as an SMMInput subclass that reads in XML file types.

The factory pattern for Operators lets SMMSim create SMMHamiltonians and

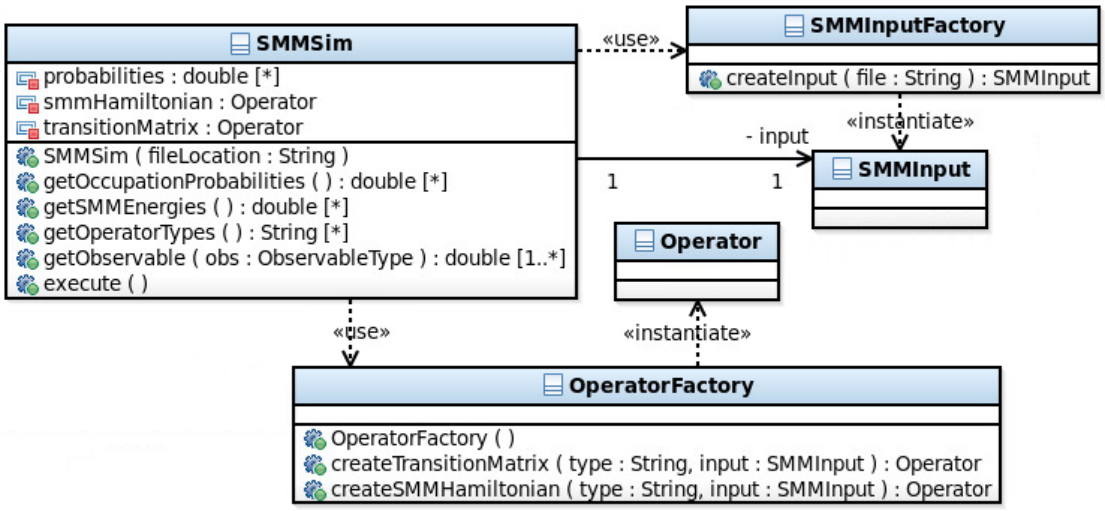

Figure 4-10: SMMSim object model, depicting dependence on input and operator factory patterns.

TransitionMatrix subclasses without direct knowledge of the underlying concrete implementation. This allows the use of the default sparse EigenOperators, or future implementations such as a PETSC Operator subclass.

The primary method SMMSim provides is *execute*, which is the entry point for simulations of electron transport across user-defined single-molecule magnets. Clients define a valid input file, which details the parameters describing the single-molecule magnet and the observable to compute, such as total current. An SMMSim instance can be created with this file, which constructs the SMMInput, SMMHamiltonian, and TransitionMatrix instances. The execute method will then take the input observable data and perform the calculation.

Chapter 5

SMMSim Results for Fe_4

To elucidate the results of our simulations for the current-voltage characteristics of Fe_4, it will be helpful to first show the case of no vibrational coupling, then follow that with our results when vibrational coupling is present. All of our simulations model Fe_4 with a neutral uniaxial magnetic anisotropy of $D = .056$ meV, a charged anisotropy of $D = .062$ meV, and a total spin $S = 5$. These initial results set the intrinsic transverse anisotropy, external magnetic fields, and molecular transport orbital energy to zero.

5.1 Results Without Vibrational Coupling

The results in the absence of vibrational coupling are shown in Figs. 5-1a, 5-1b, 5-2a, and 5-2b. These figures depict the available transitions within the bias window, the total current as a function of the applied bias, the plot of eigenstate occupation probabilities, and the total differential conductance, respectively. The gate voltage for this simulation was set to .3 meV, and at that voltage, the lowest energy state at zero bias voltage is the charged ground state $|S = 9/2, M = \pm 9/2\rangle$, as depicted in the occupation probabilities and the differential conductance plots. For low bias voltages, no transitions occur, due to the fact that there is not sufficient energy for a transition. This is a signature of the Coulomb blockade, discussed in Sec. 3.1.2 of Ch. 3. Once the bias voltage reaches a certain level, there is an increase in the current caused

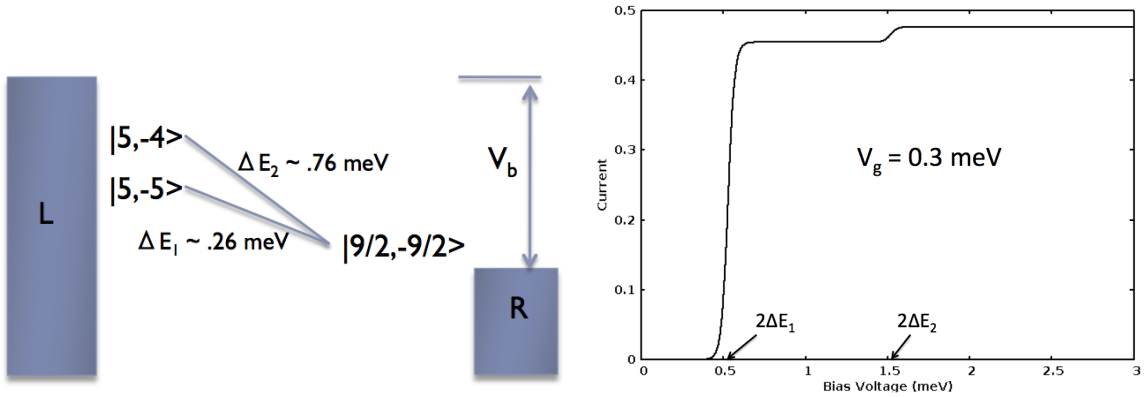

(a) (b)

Figure 5-1: Allowed transitions in the bias window (a) and current as a function of the bias voltage (b). Notice that until a valid transition state enters into the bias window, no transition occur, and thus no current can flow. Due to the symmetry of the applied bias voltage, valid transition states enter the bias window at two times the energy difference between the transitioning states, denoted here ΔE_1 and ΔE_2

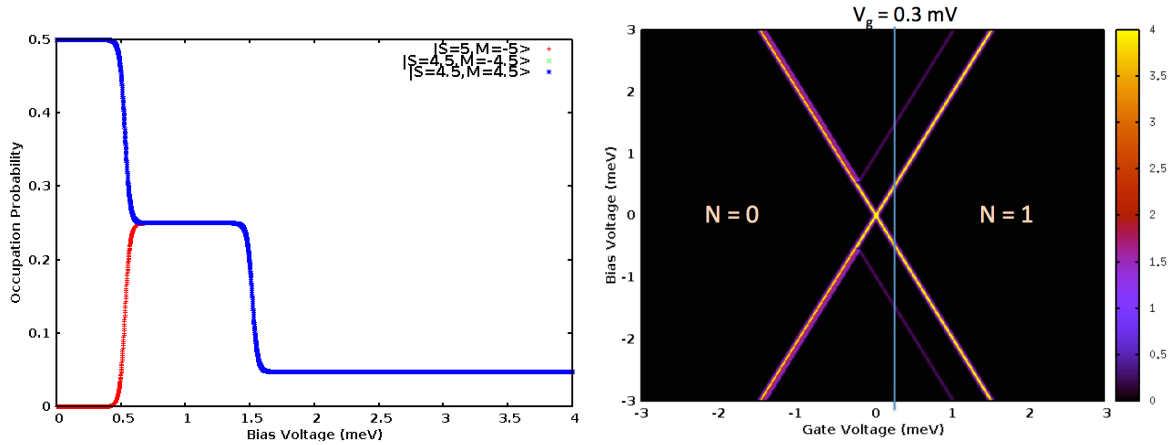

(a) (b)

Figure 5-2: Occupation probabilities (a) and differential conductance plot (b) for the case of no vibrational coupling.

by an allowed transition to the uncharged ground state $|5, -5\rangle$. In other words, at this bias voltage, the lowest unoccupied molecular orbital (LUMO) state has entered into the bias window. Due to the way we symmetrically apply the bias voltage, this jump occurs at exactly two times the energy difference between the charged and uncharged ground states. As the bias increases further, the first excited uncharged state enters into the bias window, thus allowing a second transition to occur. No further transitions can occur after that because the occupation probabilities for all states become uniform (the final flat-line in Fig. 5-2a), which implies a stagnant overall transition rate matrix.

Fig. 5-2b shows the expected Coulomb diamond, with the slanted lines representing peaks in the differential conductance. These peaks separate conducting and Coulomb blockade regions, as well as charged and uncharged states. Notice that by adjusting the gate voltage, we can modify the Coulomb blockade.

5.2 Results with Vibrational Coupling

Before we can introduce our results for the effects of vibrational coupling in Fe_4 we must detail our resultant electron-vibron couplings, λ. Using density functional theory (Ch. 2), our group has computed the vibrational modes and frequencies for the Fe_4 molecular complex [5]. That, coupled with our DFT optimized geometries for the neutral and charged Fe_4 cases, has allowed us to compute the electron-vibron coupling strengths for each of the molecular vibrational modes, in the manner discussed in Sec. 3.2.6 of Ch. 3. For our transport calculations, we only utilize those coupling strengths that are greater than one because we have found all others do not significantly contribute to the expected low bias suppression of the current. The calculated significant couplings and their corresponding frequencies are shown in Table 5.1 [5].

When we introduce molecular vibrational modes and their corresponding coupling to tunneling electrons, we see a clear suppression of the current for strong electron-vibron coupling. Fig. 5-3a shows the current as a function of the bias voltage for one normal mode with $\lambda = 1.27$ and another with $\lambda = 2.0$, and both with phonon

Electron-Vibron Coupling λ	Phonon Frequency f (cm^{-1})
1.27	16.1
1.33	20.0
1.46	30.2

Table 5.1: Computed significant electron-vibron couplings and frequencies for Fe_4 [5].

frequency $\hbar\omega = 2.0$ meV ≈ 16.1 cm^{-1}. This data was created with the same input as before, but with a gate voltage set such that the charged and uncharged ground states were degenerate at zero bias, which corresponds to $V_g = .1445$ meV. The plot shows that the overall suppression of the current increases as the electron-vibron coupling strength increases, which is expected due to the overall form of the Franck-Condon matrix elements.

The presence of vibrationally excited states in the bias window leads to more peaks in the differential conductance, shown in Fig. 5-3b. Since our charged and uncharged ground states are degenerate at zero bias, we see an immediate peak in the current. The second peak corresponds to transitions to the first excited vibrational mode $|n_v = 1\rangle$, while the third peak occurs due to transitions to the second excited vibrational mode, $|n_v = 2\rangle$. Once again, these peaks occur at exactly two times the energy difference between the ground state and the vibrational excited state ($2\hbar\omega$ for the first peak, and $4\hbar\omega$ for the second).

The stability diagram for the case of one normal mode with $\lambda = 1.27$ is shown in Fig. 5-4a, and for comparison purposes, the stability diagram for $\lambda = 3$ in Fig. 5-4b. First of all, notice the overall structure in the conducting regions of the plot. The extra peaks of differential conductance correspond to the presence of vibrationally active states within the bias window. Also, the plots show that as the strength of the electron-vibron coupling goes up, so does the characteristic low-bias suppression of the current due to the Franck-Condon blockade. We have found that this low bias suppression becomes most pronounced when $\lambda \geq 2$, which agrees with the Franck-Condon blockade predicted for a nonmagnetic molecule [15] and with the observed Franck-Condon blockade for Fe_4 [5].

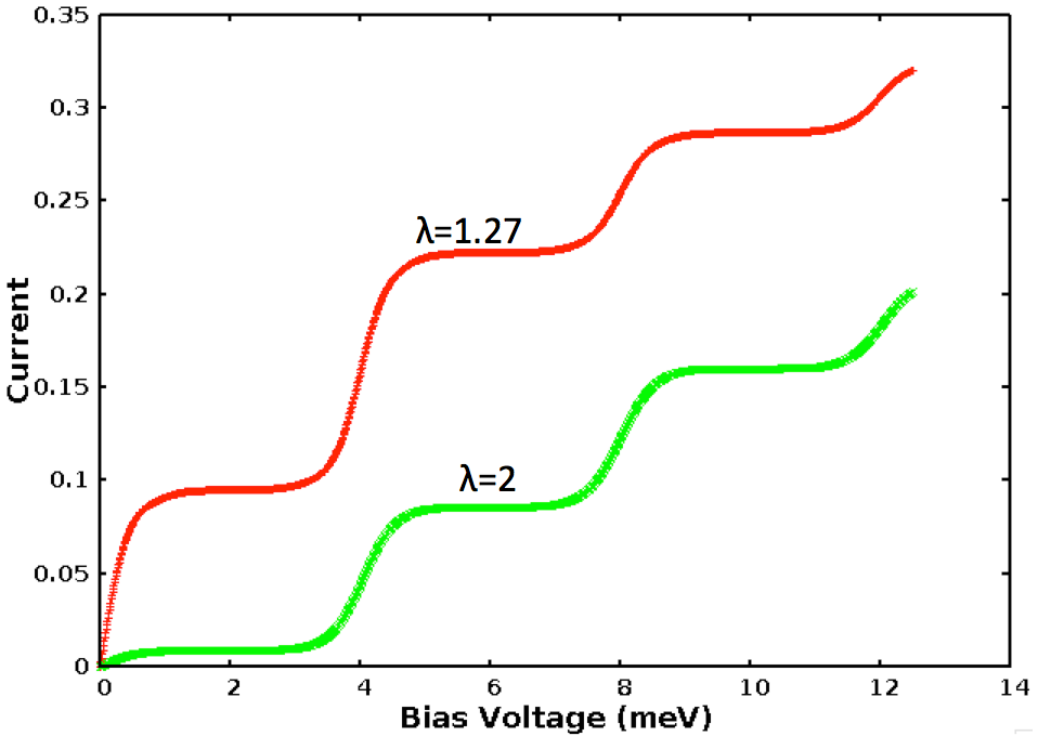

(a)

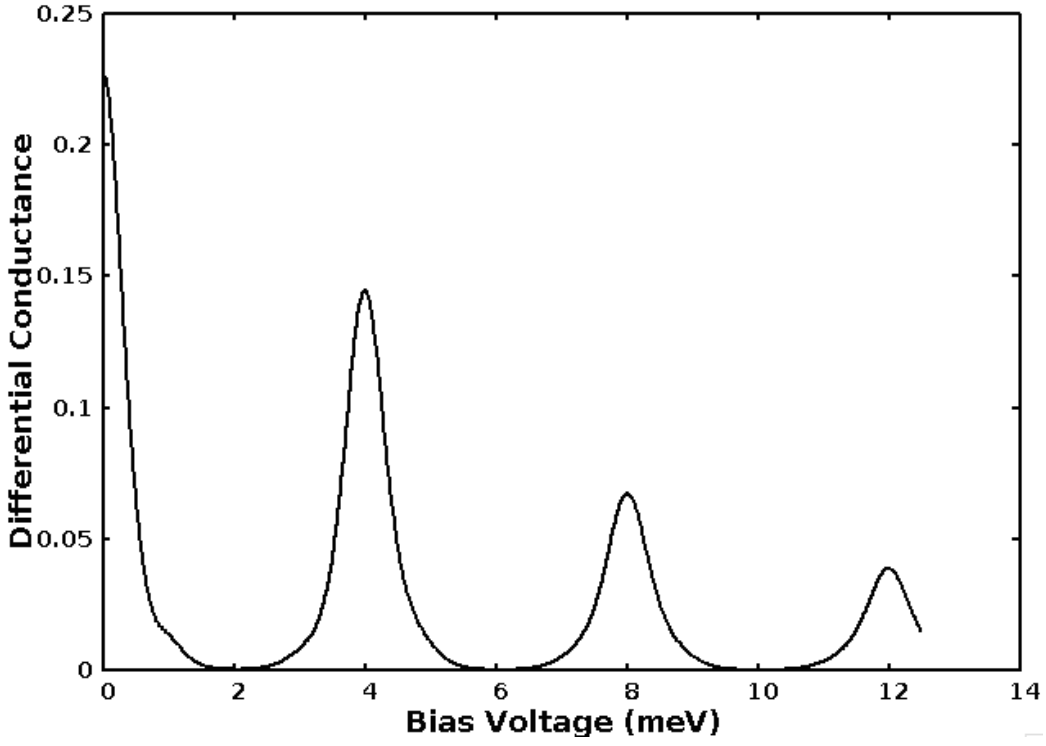

(b)

Figure 5-3: Plots of the current (a) and differential conductance (b) as a function of the bias voltage. The current shows a clear suppression of the current as the strength of the electron-vibron coupling λ increases, while the differential conductance for $\lambda = 1.27$ exhibits peaks that correspond to vibrationally allowed transitions.

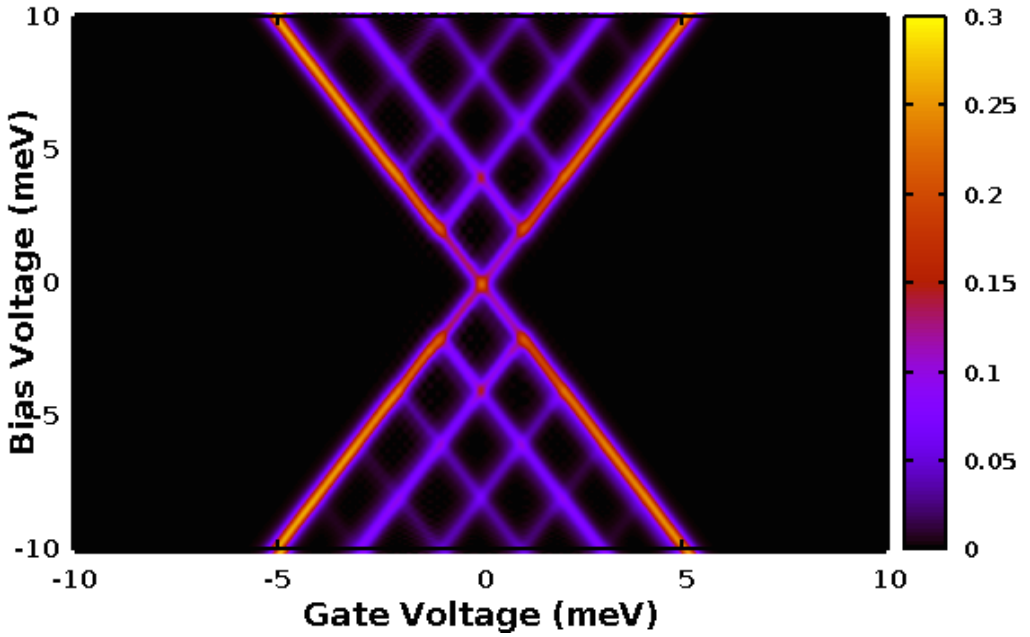

(a)

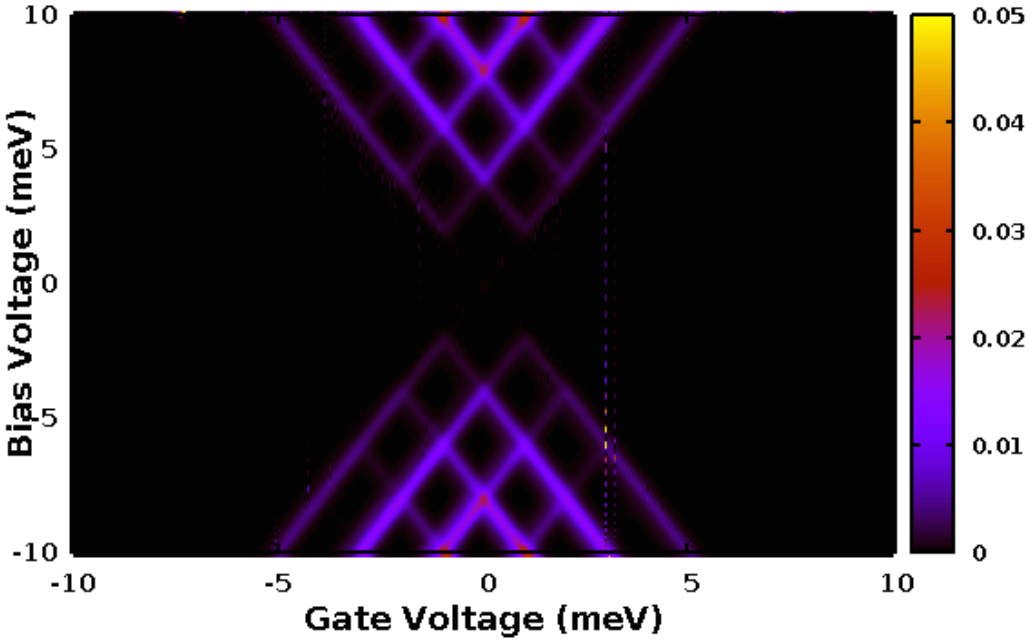

(b)

Figure 5-4: Comparison of stability plots for $\lambda = 1.27$ (a) and $\lambda = 3$ (b). A clear low-bias suppression of the current can be see in the plot for $\lambda = 3$, characteristic of the Franck-Condon blockade.

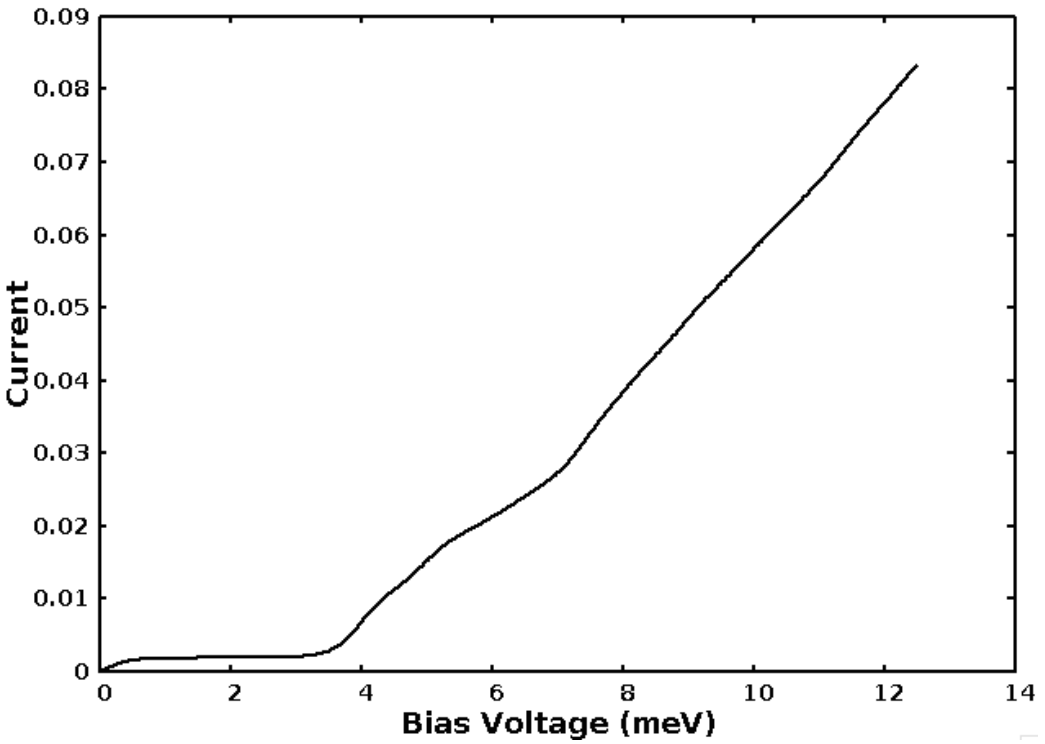

(a)

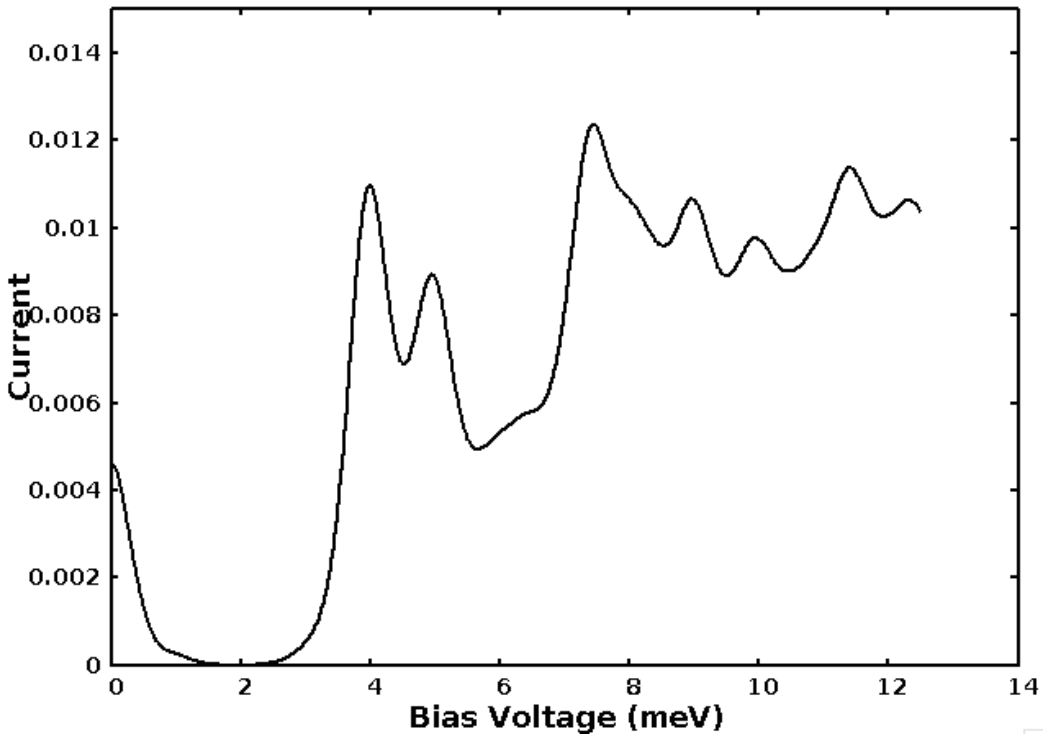

(b)

Figure 5-5: Plots of the current (a) and differential conductance (b) for the three normal modes with couplings shown in Table 5.1. The current shows a clear suppression of the current due to the combined effect of all three vibrational modes, while the differential conductance exhibits more peaks due to the presence of additional vibrationally allowed transitions.

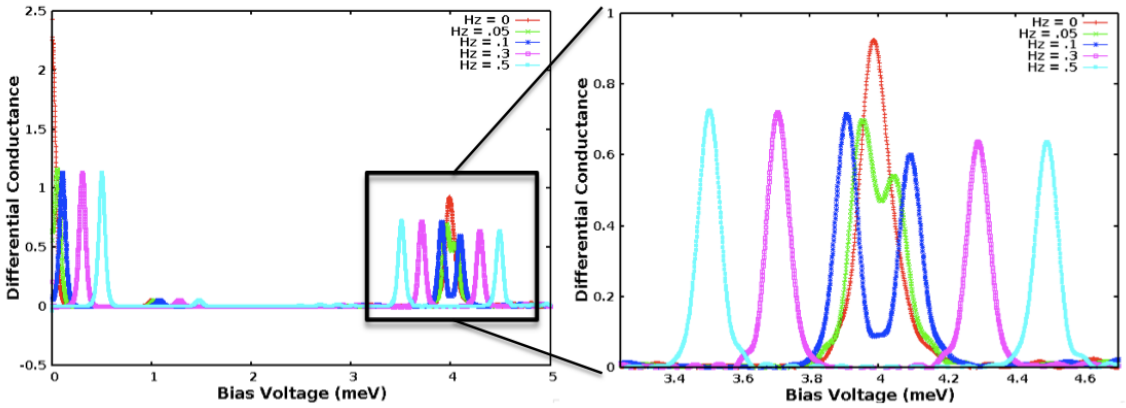

Figure 5-6: Differential conductance versus bias voltage for various external magnetic fields in the direction of the easy-axis. The plot shows a splitting of the peaks as the strength of the field increases, due to the shifting of molecular energies, as discussed in Sec. 1.2.2 of Ch. 1.

The combined effect of all three modes from Table 5.1 is shown in Figs. 5-5a, 5-5b, and they depict a large suppression of the current at low bias. The combined effort of all three electron-vibron couplings leads to the same low-bias suppression for the case of one normal mode with strong coupling strength ($\lambda \geq 2.0$). Additionally, the plots exhibit more peaks in the differential conductance due to the increase in available vibrational states in the bias window.

5.3 Effect of Easy-Axis External Field

When we turn on an external magnetic field in the direction of the easy-axis, we see further structure in the differential conductance peaks due to the energetic availability of eigenstates in the bias window. As shown in Ch. 1, the introduction of an external field acts to lower eigenstates with $M > 0$ and raise eigenstates with $M < 0$. This modification of the energy spectrum leads to the splitting of the peaks in the differential conductance, and can be seen in Fig. 5-6. When the field is off we see the same peak at 4 meV due to allowed transitions to the first excited vibrational state. As the field increases, that peak begins to split, due to the raising magnetic levels with negative M and a lowering of magnetic levels with a positive M.

Conclusion

The addition of coupling between electronic and vibrational degrees of freedom into the problem of transport across SMMs introduces a new level of complexity. This thesis has shown a methodology to handle this added complexity for the Fe_4 SMM through the use of both DFT and a model Hamiltonian and master equation approach. DFT provides a valuable tool for the calculation of molecular equilibrium geometries, which can be used in the computation of the coupling strength between the electronic and vibrational degrees of freedom in a SMM three-terminal device. This coupling strength can then be incorporated into a model Hamiltonian approach, and various system observables, such as the current as a function of the bias voltage, can be computed.

We have presented an application for the simulation of electron transport across Fe_4 in the presence of this electron-vibron coupling, called SMMSim. This code adheres to a number of software-engineering best practices, and promotes future extensibility and scalability for the addition of coupling between other degrees of freedom. It provides abstractions for quantum states and operators, as well as an efficient generator for Franck-Condon factors.

Our results using SMMSim exhibit the expected low-bias suppression of the current known as the Franck-Condon blockade. We have found that the strength of that suppression becomes more pronounced for electron-vibron coupling strengths ≥ 2.0, and under the presence of multiple vibrational modes. Additionally, the presence of external easy-axis magnetic fields leads to a splitting of the differential conductance peaks, due to a shift in the molecular energies.

References

[1] Stefania Accorsi and A. L. Barra. Tuning Anisotropy Barriers in a Family of Tetrairon(III) Single-Molecule Magnets with an S=5 Ground State. *Journal of the American Chemical Society*, (128):4742–4755, 2006.

[2] Nolan B., Brown B., Balmelli L., Bohn T., and Whali U. Model Driven Systems Development with Rational Products (IBM). http://www.redbooks.ibm.com/redbooks/pdfs/sg247368.pdf, 2008.

[3] Satish Balay, William D. Gropp, Lois Curfman McInnes, and Barry F. Smith. Efficient Management of Parallelism in Object Oriented Numerical Software Libraries. In E. Arge, A. M. Bruaset, and H. P. Langtangen, editors, *Modern Software Tools in Scientific Computing*, pages 163–202. Birkhäuser Press, 1997.

[4] E. Del Barco, a. D. Kent, S. Hill, J. M. North, N. S. Dalal, E. M. Rumberger, D. N. Hendrickson, N. Chakov, and G. Christou. Magnetic Quantum Tunneling in the Single-Molecule Magnet Mn12-Acetate. *Journal of Low Temperature Physics*, 140(1-2):119–174, July 2005.

[5] E. Burzurí, Y. Yamamoto, M. Warnock, X. Zhong, K. Park, A. Cornia, and H. S. J. van der Zant. Franck-Condon Blockade in a Single-Molecule Transistor. *Nano Letters (under review).*

[6] E. Burzurí, A. S. Zyazin, A. Cornia, and H. S. J. van der Zant. Direct Observation of Magnetic Anisotropy in an Individual Fe_4 Single-Molecule Magnet. *Phys. Rev. Lett.*, 109:147203, Oct 2012.

[7] Klaus Capelle. A Bird's-Eye View of Density Functional Theory. *Brazilian Journal of Physics*, 36(4):1318–1343, 2006.

[8] Y. Shao et. al. *Chem. Phys. 8*, pages 3172–3191, 2006.

[9] Jonathan R. Friedman and Myriam P. Sarachik. Single-Molecule Nanomagnets. *Annual Review of Condensed Matter Physics*, 1(1):109–128, August 2010.

[10] Erich Gamma, Richard Helm, Ralph Johnson, and John Vlissides. *Design Patterns: Elements of Reusable Object-oriented Software*. Addison-Wesley Longman Publishing Co., Inc., Boston, MA, USA, 1995.

[11] Gaël Guennebaud, Benoît Jacob, et al. Eigen v3. http://eigen.tuxfamily.org, 2010.

[12] P Hohenberg and W Kohn. Inhomogeneous Electron Gas. *Physical review*, 155(1962), 1964.

[13] Beck K. *Test Driven Development: By Example*. Addison-Wesley Longman Publishing Co., Inc., Boston, MA, USA, 2002.

[14] Bittner K. and Spence I. Use Case Modeling. Addison-Wesley, 2003.

[15] Jens Koch, Felix von Oppen, and A. V. Andreev. Theory of the Franck-Condon Blockade Regime. *Phys. Rev. B*, 74:205438, Nov 2006.

[16] W Kohn and L J Sham. Self-Consistent Equations Including Exchange and Correlation Effects. *Physical Review*, 140(4A):A1133–A1138, 1965.

[17] I. G. Lang and Y. A. Firsov. *Sov. Phys. JETP 16*, page 1301, 1963.

[18] Maciej Misiorny and Józef Barnaś. Spin Polarized Transport Through a Single-Molecule Magnet: Current-Induced Magnetic Switching. *Physical Review B*, 76(5):054448, August 2007.

[19] Robert G. Parr and Weitao Yang. *Density-Functional Theory of Atoms and Molecules*. Oxford University Press, New York, 1989.

[20] William H. Press, Saul A. Teukolsky, William T. Vetterling, and Brian P. Flannery. *Numerical Recipes 3rd Edition: The Art of Scientific Computing*. Cambridge University Press, New York, NY, USA, 3 edition, 2007.

[21] Peder Ruhoff. Recursion Relations for Multi-Dimensional Franck-Condon Overlap Integrals. *Chemical Physics*, 186:355–374, 1994.

[22] Peder Thusgaard Ruhoff and Mark A Ratner. Algorithms for Computing Frank-Condon Overlap Integrals. 77:383–392, 2000.

[23] Franz Schwabl. *Quantum Mechanics*. Springer, Berlin, 2nd rev. ed. edition, 1995.

[24] J. S. Seldenthuis. *Electrical and Mechanical Effects in Single-Molecule Junctions*. Gildeprint Drukkerijen, Netherlands, 2011.

[25] Johannes S Seldenthuis, Herre S J Van Der Zant, Mark A Ratner, and Joseph M Thijssen. Vibrational Excitations in Weakly Coupled Single-Molecule Junctions: A Computational Analysis. *ACS Nano*, 2(7):1445–1451, 2008.

[26] T. E. Sharp and H. M. Rosenstock. FranckCondon Factors for Polyatomic Molecules. *The Journal of Chemical Physics*, 41(11):3453, 1964.

[27] Attila Szabo. *Modern Quantum Chemistry: Introduction to Advanced Electronic Structure Theory*. Dover Publications, Mineola, N.Y, 1996.

[28] H. A. van der Vorst. BI-CGSTAB: A Fast and Smoothly Converging Variant of BI-CG for the Solution of Nonsymmetric Linear Systems. *SIAM J. Sci. Stat. Comput.*, 13(2):631–644, March 1992.

[29] W. Wernsdorfer. *Advanced Magnetic Nanostructures*, chapter 6: Molecular Nanomagnets. Springer, New York, NY, 2006.

[30] W. Wernsdorfer, R. Sessoli, A. Caneschi, D. Gatteschi, and A. Cornia. Nonadiabatic Landau-Zener Tunneling in Fe_8 Molecular Nanomagnets. *EPL (Europhysics Letters)*, 50(4):552, 2000.

[31] Qin Wu and Troy Van Voorhis. Direct Optimization Method To Study Constrained Systems Within Density-Functional Theory. *Phys. Rev. A*, 72:024502, Aug 2005.